Technical Report Documentation Page

1. Report No.	2. Government Accession No.	3. Recipient's Catalog No.
TX-98/987-S		

4. Title and Subtitle	5. Report Date
FINAL REPORT ON THE LONG-RANGE REHABILITATION PLAN FOR US 59 IN THE LUFKIN DISTRICT OF TEXAS	September 1998
	6. Performing Organization Code
7. Author(s) Chiu Liu, Terry Dossey, and B. Frank McCullough	8. Performing Organization Report No. 987-S
9. Performing Organization Name and Address Center for Transportation Research The University of Texas at Austin 3208 Red River, Suite 200 Austin, TX 78705-2650	10. Work Unit No. (TRAIS) 11. Contract or Grant No. Project 7-987
12. Sponsoring Agency Name and Address Texas Department of Transportation Research and Technology Transfer Section/Construction Division P.O. Box 5080 Austin, TX 78763-5080	13. Type of Report and Period Covered Project Summary Report (9/96-8/97) 14. Sponsoring Agency Code

15. Supplementary Notes

Project conducted in cooperation with the Texas Department of Transportation.

16. Abstract

In this report, we briefly introduce Project 7-987 and then describe what we intend to do in the future with US 59. We have organized US 59 traffic data in terms of Texas Department of Transportation (TxDOT) classified sections, the pavement types defined previously in CTR Report 987-1, and the mile markers along the roadway. A general logistic model for the development of reflective and fatigue cracks in pavement surface is proposed and verified using the information collected during the last eight conditions surveys of the test sections. The rut depth data along the wheelpaths in various test sections are found to follow the Gamma distribution. The raw average rut depth for various test sections have been plotted against the amount of traffic loadings placed on the pavement. The irregular behavior of the rut data is observed for various test sections in the first 2-year period. Analytic models predicting development of reflective cracks, fatigue cracks, and rut depth in pavement surfaces are calibrated using the field data. Then, two computer programs, one for flexible pavement and the other for rigid pavement, are generated for use in planning the future rehabilitation of US 59. Examples using the programs are demonstrated and reasonable results are obtained. Overlay strategies for different control sections along US 59 are proposed based on the AADT information.

17. Key Words	18. Distribution Statement
Pavement rehabilitation, Lufkin District, US 59, overlay strategies, cracking distress modeling	No restrictions. This document is available to the public through the National Technical Information Service, Springfield, Virginia 22161.

19. Security Classif. (of report)	20. Security Classif. (of this page)	21. No. of pages	22. Price
Unclassified	Unclassified	82	

FINAL REPORT ON THE LONG-RANGE REHABILITATION PLAN FOR US 59 IN THE LUFKIN DISTRICT OF TEXAS

by

Chiu Liu,

Terry Dossey,

and

B. Frank McCullough

Project Summary Report Number 987-S

Research Project 7-987

A Long-Range Plan for the Rehabilitation of US 59 in the Lufkin District

Conducted for the

TEXAS DEPARTMENT OF TRANSPORTATION

by the

CENTER FOR TRANSPORTATION RESEARCH

Bureau of Engineering Research

THE UNIVERSITY OF TEXAS AT AUSTIN

September 1998

IMPLEMENTATION RECOMMENDATIONS

The condition surveys carried out over the last 5 years for cracking and rutting distress on the test sections in the Texas Department of Transportation's Lufkin District are organized and presented in this report. Using weigh-in-motion (WIM) data collected in the Lufkin District, a finite element model for rigid pavements used in a previous Project 7-987 report, and the ELSYM model for flexible pavements, we have calibrated cracking and rutting models for overlays on rigid and flexible pavements, respectively. Taking into account user costs, computer programs for overlays on rigid or flexible pavements have been generated for use in planning future rehabilitation in the Lufkin District.

The optimum overlay strategies presented in the implementation recommendations of Chapter 6 (page 69) represent a planning document for estimating the funding required to maintain US 59 in an acceptable condition for the next 50 years.

ACKNOWLEDGMENTS

The researchers acknowledge the expert assistance provided by the Texas Department of Transportation project director, Mr. E. Starnator (Lufkin District).

Prepared in cooperation with the Texas Department of Transportation.

DISCLAIMERS

The contents of this report reflect the views of the authors, who are responsible for the facts and the accuracy of the data presented herein. The contents do not necessarily reflect the official views or policies of the Texas Department of Transportation. This report does not constitute a standard, specification, or regulation.

There was no invention or discovery conceived or first actually reduced to practice in the course of or under this contract, including any art, method, process, machine, manufacture, design or composition of matter, or any new and useful improvement thereof, or any variety of plant, which is or may be patentable under the patent laws of the United States of America or any foreign country.

NOT INTENDED FOR CONSTRUCTION,
BIDDING, OR PERMIT PURPOSES

B. Frank McCullough, P.E. (Texas No. 19914)
Research Supervisor

TABLE OF CONTENTS

SUMMARY

In this report, we briefly introduce Project 7-987 and then describe what we intend to do in the future with US 59. We have organized US 59 traffic data in terms of Texas Department of Transportation (TxDOT) classified sections, the pavement types defined previously in CTR Report 987-1, and the mile markers along the roadway. A general logistic model for the development of reflective and fatigue cracks in pavement surface is proposed and verified using the information collected during the last eight conditions surveys of the test sections. The rut depth data along the wheelpaths in various test sections are found to follow the Gamma distribution. The raw average rut depth for various test sections have been plotted against the amount of traffic loadings placed on the pavement. The irregular behavior of the rut data is observed for various test sections in the first 2-year period. Analytic models predicting development of reflective cracks, fatigue cracks, and rut depth in pavement surfaces are calibrated using the field data. Then, two computer programs, one for flexible pavement and the other for rigid pavement, are generated for use in planning the future rehabilitation of US 59. Examples using the programs are demonstrated and reasonable results are obtained. Overlay strategies for different control sections along US 59 are proposed based on the AADT information.

CHAPTER 1. INTRODUCTION

BACKGROUND

US 59 within the Lufkin District represents one of the busiest highways in Texas. It is a principal arterial that runs from Laredo through Houston and Lufkin, exits Texas at Texarkana, and then extends northeast all the way to Canada. Within the Lufkin District, it traverses Shelby, Nacogdoches, Angelina, Polk, and San Jacinto counties (dubbed the SNAPS counties) from the northern to the southern border of the Texas Department of Transportation (TxDOT) district. The total length of US 59 within the district is about 193 km (120 miles). The cross sections of US 59 vary from northern Shelby County to southern San Jacinto County. Within the Lufkin District, the roadway itself is constructed of approximately seven types of flexible pavement and thirteen types of rigid pavement (see CTR Report 987-1).

Given the key role that this highway plays in moving much NAFTA-generated truck traffic, TxDOT, in cooperation with the Center for Transportation Research (CTR) of The University of Texas at Austin, initiated Project 7-987 to develop a long-range rehabilitation plan for US 59 in the Lufkin District.

PROJECT 987 ACCOMPLISHMENTS

For the overall Project 987 effort, the CTR team has accomplished the following:

(1) Classified geometric cross sections of US 59 within the Lufkin District. As part of this task, the study team also identified the roadway's main pavement distresses by performing comprehensive condition surveys throughout the district. This survey then provided the basis for constructing test sections in the district (Hoskins et al., CTR Report 987-1);
(2) Investigated the effects of work zone detours set up during the construction of the test section in the district (Lee and Ahmad, CTR Report 987-2);
(3) Tabulated and reported the construction costs for the fourteen test sections constructed using various recipes in the district (Allison and McCullough, CTR Report 987-3);
(4) Documented the results obtained from six condition surveys of pavement distress observed on the test sections; the study team then backcalculated the stiffness for each layer of the fourteen test sections (Cho et al., CTR Report 987-4);
(5) Reported preliminary findings on traffic-load forecasting using weigh-in-motion (WIM) data collected at two test-section WIM sites (Lee and Pangburn, CTR Report 987-5);
(6) Investigated the use of other statistical techniques for forecasting traffic loading using WIM data (Qu et al., CTR Report 987-6);

(7) Examined potential rehabilitation strategies using an FEM (finite element method) and by investigating the thermal and traffic loading effects on pavement response (Cho et al., CTR Report 987-7);
(8) Analyzed the WIM data and documented the recorded test-section ambient and pavement surface temperature (Lee and Garner, CTR Report 987-8); and
(9) Generated a rehabilitation plan for US 59 in the Lufkin District (Liu et al., CTR Report 987-9).

For transportation planners in the Lufkin District, a key question that has provoked much of the project's activity has been: How can the district make the best use of existing pavements? In an effort to provide a practical answer to the question, personnel from TxDOT and CTR formed a task group to identify existing roadway problems. Traffic data collection, pilot condition surveys, and deflection testing along US 59 in the Lufkin District were undertaken as part of this effort. Based on the collected data, a plan for constructing experimental sections was prepared. Seven overlay sections using different construction recipes for the jointed rigid pavement north of Corrigan, along with seven overlay sections south of Corrigan, were constructed in 1992. Each of the sections is 305 m (1,000 ft) in length.

The original jointed rigid pavement, which has a 228.6 x 177.8 x 228.6 mm (9 x 7 x 9 in.) cross section, was constructed in 1943 and, since then, has been resurfaced with 38.1 mm (1.5 in.), 38.1 mm (1.5 in.), 30.48 mm (1.2 in.), 33.02 mm (1.3 in.), and 38.1 mm (1.5 in.) of asphalt concrete in 1953, 1964, 1971, 1979, and 1982, respectively. Altogether, a total of 177.8 mm (7 in.) of asphalt concrete has been placed on the rigid pavement prior to the construction of the test sections. The existing flexible pavement, constructed in 1966, is comprised of a 152.4 mm (6 in.) lime-treated subgrade, a 152.4 mm (6 in.) cement-treated base, a 114.3 mm (4.5 in.) black base, and 38.1 mm (1.5 in.) of asphalt concrete; it has also been resurfaced with asphalt concrete several times. The depth of the surface layer of the flexible pavement — again, prior to the construction of the test sections — is approximately 279.4 mm (11 in.) (Allison et al., CTR Report 987-3). The cross sections of the test sections are shown in Figures 1.1 and 1.2. Observations and condition surveys of the distress appearing on the surfaces of the test sections have been carried out over the last 4.5 years by CTR staff. Many sets of distress maps and rut depth data for the test sections have been generated.

RIGID PAVEMENT OVERLAY CONSTRUCTION

After the accumulation of 177.8 mm (7 in.) of asphalt concrete overlay was removed and the jointed rigid pavement repaired, section R1 was constructed using 101.6 mm (4 in.) of Type C asphalt concrete. R1 turns out to be an ineffective strategy in combating cracking distress.

Once the existing 177.8-mm (7-in.) asphalt concrete overlay was removed and the jointed rigid pavement hammered into pieces using a Woergten drop hammer, section R2 was then surfaced using 101.6 mm (4 in.) of Type C asphalt concrete for the first 152.4 m (500 ft) of the section, and then 139.7 mm (5.5 in.) of Type C asphalt concrete for the rest of the section. Overall, section R2 performed poorly in terms of fatigue cracking, although the crack and seat method was applied for preventing reflective cracks.

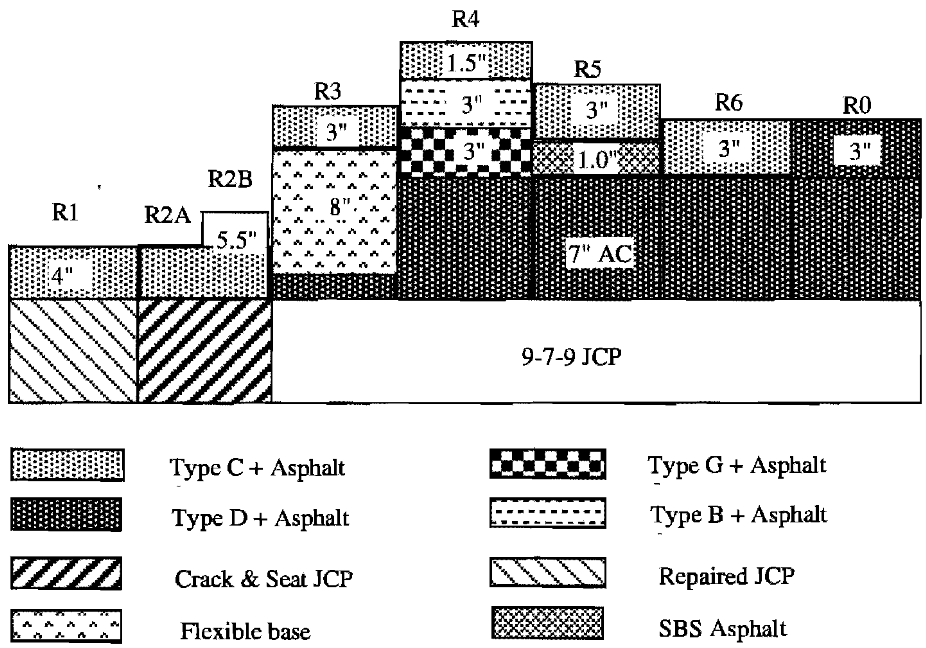

Figure 1.1: Overlay cross sections for rigid pavement (Note: 1 in.=25.4 mm).

Section R3 was constructed by first milling off 139.127 mm (5 in.) of the existing 177.8 mm (7 in.) asphalt concrete and then placing 203.2 mm (8 in.) of flexible base on top of the remaining asphalt concrete layer. R3 set up then involved placing 76.2 mm (3 in.) of Type C asphalt concrete on top of the 203.2 mm (8 in.) flexible base.

Section R4 was constructed by first placing 76.2 mm (3 in.) of Type G asphalt concrete on top of the existing pavement, then 76.2 mm (3 in.) of Type B asphalt concrete on top of the Type G materials, and, finally, 38.1 mm (1.5 in.) of Type C asphalt concrete on the surface. R4 was thus an expensive section; it was designed to retard reflective cracking by placing the relatively large G-Type aggregates in direct contact with the pervious asphalt concrete. As our observations indicated, the recipe used for this section proved effective in slowing down the process of reflective cracking.

Section R5 was constructed by placing 76.2 mm (3 in.) of Type C asphalt concrete on top of the 25.4 mm (1 in.) of styrene-Butadiene-styrene (SBS) asphalt material. The SBS also proved to be an effective agent in fighting reflective cracks. Finally, sections R6 and R0 were constructed by placing 76.2 mm (3 in.) Type C and 76.2 mm (3 in.) Type D asphalt concrete on top of the existing roadway, respectively. R0, which served as the control section, was set up using conventional Type D material.

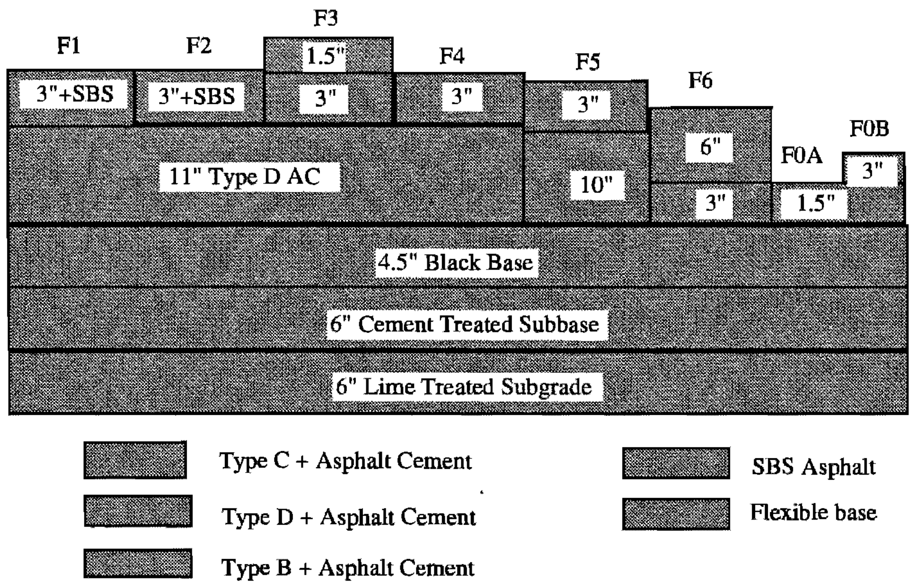

Figure 1.2: Overlay cross sections for flexible pavements.

FLEXIBLE PAVEMENT OVERLAY CONSTRUCTION

This section describes the construction recipes used for the flexible pavement overlays. Section F1 was constructed using 76.2 mm (3 in.) of Type D asphalt concrete blended with the SBS polymer. (In combating cracking distress, section F1 outperformed conventionally constructed control section F0.) Section F2 was constructed by placing 76.2 mm (3 in.) Type C SBS-modified asphalt concrete on top of the existing pavement. Among the seven selected overlay recipes for the flexible pavement, F2 proved to be the least expensive as well as the best recipe for preventing fatigue and reflective cracking.

Section F3 was set up by placing 38.1 mm (1.5 in.) of Type C asphalt concrete on top of 76.2 mm (3 in.) of Type G asphalt concrete. Section F4 was constructed by first placing 76.2 mm (3 in.) of Type G asphalt concrete on top of the existing pavement, then 76.2 mm (3 in.) of Type B asphalt concrete on top of the Type G materials, and, finally, 38.1 mm (1.5 in.) of Type C asphalt concrete on the surface. Recipe F4 proved somewhat effective in combating reflective cracking.

Section F5 was constructed by first milling off the existing 279.4 mm (11 in.) asphalt concrete surface layer (CTR Report 987–3) and then placing 76.2 mm (3 in.) of Type C asphalt concrete on top of a 254.0 mm (10 in.) flexible base material that is on top of the existing asphalt pavement. Section F5 proved to be the poorest performer among the seven flexible sections, exhibiting as it did deep rut depth and rapid crack growth on the overlay surface.

Section F6 was constructed by first clearing off the existing 279.4 mm (11 in.) of asphalt concrete surface layer; 76.2 mm (3 in.) of Type G asphalt concrete was then placed on the existing flexible base and 152.4 mm (6 in.) Type C asphalt concrete was placed on top of the Type G asphalt concrete. F6, the most expensive section constructed, proved to be the best performer in terms of rutting and cracking performance. Finally, control section F0 was set up using conventional Type D material.

REPORT ORGANIZATION

Chapter 2 presents the traffic flow information (by county) recorded over the last 10 years within the Lufkin District. Chapter 3 then describes the attempt to model the evolution of surface cracking distress based on the information collected from the test-section overlays. In Chapter 4, we use the finite element model for rigid pavement overlays presented in previous Project 7-987 reports and the ELSYM layer model for overlays on flexible pavements to estimate the tensile strain and the vertical strain existing along the interface between the overlay and the overlaid pavement. By correlating the observed rut depth distress and the area of cracking distress with the vertical and tensile strain along the interface, respectively, we generate the prediction models for cracking and rutting distress, respectively; this then enables us to estimate the terminal (failure) traffic loading associated with an overlay using a specific construction recipe. In addition, the chapter discusses the dependence of the number of terminal loadings associated with the test sections' present serviceability index (PSI) on the thickness of an overlay. In Chapter 5, we present the rehabilitation computer programs generated based on the phenomenological distress models calibrated using the data collected for the test sections. Finally, a summary and recommendations are provided in Chapter 6.

CHAPTER 2. TRAFFIC FLOW INFORMATION

The SNAPS counties' traffic information for the last 10 years or so is classified according to TxDOT section numbers associated with US 59. In this chapter, we present tables of traffic flow information relevant to each county. The tables include traffic growth rates, pavement section numbers, pavement types (as classified in Report 987-1), and the marker system, which might to some extent be helpful to the district. Other tables tabulate the traffic information collected over the past 10 years or so up to 1994, according to the section numbers employed by TxDOT.

Table 2.1: Sections, markers, AADT, and growth rate for Shelby Co.

Shelby Co. 210										
C.S.	**B.M.**	**E.M.**	**B.R.M.**	**E.R.M.**	**B.R.F.D.**	**E.R.F.D.**	**AADT (94)**	**(NB)**	**(SB)**	**Growth rate (%)**
63-06	0.000	1.851	326	326	0	1.851	7500	R9	F1	-0.023
	1.851	2.000	326	328	1.851	0.163	7300	R9	F1	0.585
175-2	0.000	1.412	328	328	0.163	1.575	5900	N.A.	N.A.	-2.900
175-4	0.000	6.486	328	336	1.412	0.061	6000	R11	R11	0.893
	6.486	7.696	336	336	0.061	1.271	5900	R11	R11	0.182
	7.696	8.361	336	336	1.271	1.875	6000	R11	R11	-1.820
	8.361	8.776	336	338	1.875	0.351	6600	R11	R11	-0.386
175-5	0.121	0.464	338	338	0.351	0.718	8700	F4	F4	0.340
	0.464	0.789	338	338	0.718	1.066	8300	F4	F4	1.411
	0.789	2.090	338	340	1.066	0.429	7100	F4	F4	1.614
	2.090	5.308	340	342	0.429	1.647	6200	R13	R13	0.657

Table 2.2: AADT and growth rate for the last 10 years for Shelby Co.

	Growth (.023) Section 63-6	Growth (0.585) 63-6-end	Growth (-2.9) Section 175-2	Growth (.893) Section 174-4-1	Growth (.182) Section 175-4-2	Growth (-1.82) Section 175-4-3	Growth (-0.386) Section 175-4-4	Growth (0.340) Section 175-5-1	Growth (1.411) Section 175-5-2	Growth (1.614) Section 175-5-3
Year	**AADT**	**AADT**	**AADT**	**AADT**	**AADT**	**AADT**	**AADT**	**AADT**	**AADT**	**AADT**
1994	7500	7300	5900	6000	5900	6000	6600	8700	8300	7100
1993	7400	7200	6000	6300	6500	6100	6800	8900	8700	7100
1992	7600	7300	8000	5800	5900	5500	6900	8800	8600	6600
1991	7200	6900	8500	5100	5400	5300	7400	7700	7700	6200
1990	6900	7000	8600	5200	5800	5600	6800	7500	8000	6100
1989	7000	6800	8400	5300	5900	5800	6400	8200	8000	6000
1988	7100	6700	8200	5300	5500	5400	6200	7300	7900	5800
1987	7600	7000	8400	5500	5900	6700	7100	8500	8000	6200
1986	7600	7200	8200	6100	6300	7100	7500	8900	7800	6500
1985	7400	6800	7800	5300	5800	6600	6900	8400	7200	6000

Table 2.3: Sections, markers, AADT, and growth rate for Nacogdoches Co.

Nacogdoches Co. 174										
C.S.	**B.M.**	**E.M.**	**B. R. M.**	**E. R. M.**	**B.R.F.D.**	**E.R.F.D.**	**AADT**	**(NB)**	**(SB)**	**Growth rate (%)**
175-6	0.000	1.300	346	346	0.000	1.300	6700	R13	R13	1.86
	1.300	1.463	346	346	1.300	1.463	6700	R8	R8	1.86
	1.463	1.772	346	346	1.463	1.772	7800	R8	R8	-0.57
	1.772	1.842	346	346	1.772	1.842	8800	R8	R8	0.94
	1.842	2.547	346	348	1.842	0.547	8600	R8	R8	1.30
	2.547	2.689	348	348	0.547	0.689	7500	R8	R8	1.57
	2.689	2.800	348	348	0.693	0.800	7500	R8	R8	1.57
	2.800	5.630	348	350	0.800	1.630	7500	F4	F4	1.57
175-7	5.630	11.714	350	356	0.800	1.714	7500	F4	F4	1.10
	11.714	15.300	356	360	1.714	1.298	8600	F4	F4	1.80
	15.300	16.000	360	360	1.298	1.998	8600	F4	F1?	1.80
	11.714	16.145	356	362	·1.714	0.135	8600	F4	F1?	1.80
2560-1	1.990	3.196	362	362	0.135	1.226	13600			3.98
	1.990	3.196	362	362	0.135	1.226	13600	F4	F1	3.98
	3.196	4.905	362	364	1.226	0.867	19700	F4	F1	4.75
	4.905	5.500	364	364	0.867	1.450	19100	F4	F1	3.76
	5.500	7.049	364	366	1.450	1.066	19100	F4	F4	3.76
	7.049	7.550	366	366	1.066	1.530	18800	F4	F4	3.93
	7.550	8.169	366	368	1.530	0.218	18800	F2	F4	3.93
	8.169	9.027	368	368	0.218	1.076	19800	F2	F5	4.48
	9.027	9.795	368	368	1.076	1.844	17260	F2	F5	3.88
	23.781	29.970	368	376	1.844	0.009	25000			2.75
	23.781	26.000	368	370	0.010	2.205	25000	F1	F1	2.75
	26.000	27.300	370	372	2.205	1.250	25000	R7	F4	2.75
	27.300	29.970	372	376	1.250	0.009	25000	R7	R6	2.75
	29.970	31.400	376	376	0.009	1.439	19300	R7	R6	2.94
	31.400	32.894	376	378	1.439	1.074	19300	R6	F4	2.94

Table 2.4: AADT and growth rate for the last 10 years for Nacogdoches Co.

	Growth (1.86) Section 175-6-1	**Growth (-0.572) Section 175-6-2**	**Growth (0.936) Section 175-6-3**	**Growth (1.3) Section 175-6-4**	**Growth (1.57) Section 175-6-5**	**Growth (1.1) Section 175-7-1**	**Growth (1.8) Section 175-7-2**	**Growth (3.98) Section 2560-1-1**	**Growth (4.75) Section 2560-1-2**	**Growth (3.76) Section 2560-1-3**
Year	**AADT**	**AADT**	**AADT**	**AADT**	**AADT**	**AADT**	**AADT**	**AADT**	**AADT**	**AADT**
1994	6700	7800	8800	8600	7500	7500	8600	13600	19700	19100
1993	6600	7800	8700	8500	7200	7100	8200	13300	19100	20000
1992	6800	7500	8000	8500	7000	7500	8000	13500	17000	16800
1991	6200	8500	9400	8800	7100	7600	8200	14400	17500	17200
1990	5700	8300	8200	8100	6600	7100	7400	12000	17700	17200
1989	5500	8200	8000	7900	6300	6800	7000	11200	15300	15400
1988	5500	8200	8200	7500	6400	6500	7400	10700	14500	15500
1987	5900	8600	8600	8100	6600	6900	7400	10700	14300	15000
1986	6000	8100	8100	7900	6700	7100	7500	10200	13200	13900
1985	5800	7900	7900	7800	6400	6800	7200	10200	13100	14200

	Growth (3.93) Section 2560-1-4	**Growth (4.48) Section 2560-1-5**	**Growth (3.88) Section 2560-1-6**	**Growth (2.75) Section 176-1-1**	**Growth (2.94) Section 176-1-2**
Year	**AADT**	**AADT**	**AADT**	**AADT**	**AADT**
1994	18800	19800	17260	25000	19300
1993	18500	18100	17400	24000	18600
1992	15900	15600	16200	21000	17800
1991	17000	16200	14800	20000	17400
1990	16800	16600	14900	22000	17100
1989	15000	14800	14000	21000	16200
1988	14900	14800	13500	20000	16200
1987	14000	14400	13400	22000	15400
1986	13200	13400	12700	19200	15200
1985	13500	12000	12500	17600	14700

Table 2.5: Sections, markers, AADT, and growth rate for Angelina Co.

Angelina Co. 174										
C.S.	B.M.	E.M.	B. R. M.	E. R. M.	B.R.F.D.	E.R.F.D.	AADT	(NB)	(SB)	Growth rate (%)
176-2	0.000	1.232	378	380	1.074	1.216	19300	F4	R6	2.45
	1.232	1.600	380	380	1.216	1.584	22000	R6	R6	2.57
	1.600	2.900	380	382	1.584	0.920	22000	R4	R8	2.57
	2.900	3.900	382	382	0.920	1.920	22000	R6	R6	2.29
	3.900	4.600	382	384	1.920	0.600	22000	R8	R8	2.29
	4.600	5.300	384	384	0.600	1.300	22000	R4?	R4?	2.06
	5.300	6.033	384	386	1.300	0.500	22000	R4?	R4?	2.06
	1.232	6.033	380	386	1.238	0.033	22000			2.06
	9.976	10.443	386	386	0.033	0.467	22000	R4?	R4?	5.32
2553-1	10.443	11.543	386	387	0.467	0.543	22000	F6	F6	5.32
	11.543	12.467	387	388	0.543	0.467	30000	F6?	F6?	7.52
	12.467	12.687	388	388	0.467	0.687	30000	F6?	F6?	5.96
	12.687	13.230	388	389	0.687	0.230	27510	F7?	F7?	4.58
	13.230	13.243	389	389	0.230	0.243	32000	F7?	F7?	5.88
	13.243	14.131	389	390	0.243	0.131	32000	F7	F7	5.88
	14.131	14.831	390	390	0.131	0.831	33000	F7	F7	6.32
	14.831	15.143	390	390	0.131	0.831	32530	F7	F7	5.73
	15.143	15.900	390	391	0.831	0.900	32530	R4	R6	5.73
176-3	1.240	3.202	391	392	0.900	0.542	40000	R4	R6	3.55
	3.202	6.568	392	394	0.542	1.884	24000	R4	R6	3.77
	6.568	7.664	394	396	1.884	1.010	25000	R4	R6	3.58
	7.664	8.083	396	396	1.010	1.429	24000	R4	R6	2.12
	8.083	9.221	396	398	1.429	0.567	24000	R6	R4	2.12
	9.221	9.383	398	398	0.567	0.729	23000	R6	R4	1.89
	9.383	9.483	398	398	0.729	0.829	23000	R6	R6	1.89
	9.483	10.420	398	398	0.829	1.766	23000	R4	R6	1.89
	10.420	10.738	398	400	1.766	0.084	21000	R4	R6	1.57
	10.738	11.278	400	400	0.084	0.624	19700	R4	R6	2.37
	11.278	12.483	400	400	0.624	1.829	16700	R4	R6	2.51
	12.483	12.683	400	402	1.829	0.029	16700	R4	?	2.51
	11.278	14.616	400	402	0.624	1.962	16700			2.51

Table 2.6: AADT and growth rate for the last 10 years for Angelina Co.

	Growth (2.45) Section 176-2-1	Growth (2.57) Section 176-2-2	Growth (2.29) Section 176-2-3	Growth (2.06) Section 176-2-4	Growth (5.32) Section 2553-1-1	Growth (7.52) Section 2553-1-2	Growth (5.96) Section 2553-1-3	Growth (4.58) Section 2553-1-4	Growth (5.88) Section 2553-1-5	Growth (6.32) Section 2553-1-6
Year	**AADT**	**AADT**	**AADT**	**AADT**	**AADT**	**AADT**	**AADT**	**AADT**	**AADT**	**AADT**
1994	19300	22000	22000	22000	22000	30000	30000	27510	32000	33000
1993	18600	22000	23000	23000	23000	28000	28000	30000	31000	32000
1992	17800	18400	20000	22000	16000	21000	23000	26000	27000	28000
1991	17400	18000	19000	20000	14600	21000	25000	27000	27000	27000
1990	17100	18000	19000	18800	13900	20000	23000	25000	25000	26000
1989	16100	17200	18800	20000	13400	19600	22000	24000	24000	24000
1988	16100	17700	19000	20000	14400	16900	19600	23000	22000	22000
1987	15300	17400	18300	19100	14000	16900	19200	22000	21000	21000
1986	15200	17000	18400	19000	14200	14900	17200	19400	19800	19900
1985	16200	17500	18100	18800	13100	15000	17700	19400	19100	19000
	Growth (5.73) Section 2553-1-7	**Growth (3.55) Section 176-3-1**	**Growth (3.77) Section 176-3-2**	**Growth (3.58) Section 176-3-3**	**Growth (2.12) Section 176-3-4**	**Growth (2.12) Section 176-3-5**	**Growth (1.89) Section 176-3-6**	**Growth (1.57) Section 176-3-7**	**Growth (2.37) Section 176-3-8**	**Growth (2.51) Section 176-3-9**
Year	**AADT**	**AADT**	**AADT**	**AADT**	**AADT**	**AADT**	**AADT**	**AADT**	**AADT**	**AADT**
1994	32530	40000	24000	25000	24000	24000	23000	21000	19700	16700
1993	33000	37000	23000	24000	19800	19800	22000	20000	19400	16900
1992	32000	35000	21000	22000	22000	22000	21000	20000	17700	16000
1991	30000	33000	19300	22000	21000	21000	20000	19100	17300	14600
1990	28000	30000	19000	20000	20000	20000	21000	20000	16700	13900
1989	27000	30000	17100	18600	19000	19000	20000	19200	16200	13400
1988	24000	32000	18200	19500	19700	19700	20000	19000	17200	14400
1987	23000	31000	17600	18800	19000	19000	19300	18400	16700	14000
1986	21000	28000	16900	18500	18900	18900	19400	18400	16400	14200
1985	21000	28000	17400	18200	18800	18800	18900	17700	15100	13100

Table 2.7: Sections, markers, AADT, and growth rate for Polk Co.

Polk Co. 174										
C.S.	**B.M.**	**E.M.**	**B. R. M.**	**E. R. M.**	**B.R.F.D.**	**E.R.F.D.**	**AADT**	**(NB)**	**(SB)**	**Growth rate (%)**
176-4	0.000	2.548	404	406	0.000	0.548	16700			2.51
	0.000	2.548	404	406	0.000	0.548	16700	F3?	R2	3.82
	2.548	2.900	406	406	0.548	0.900	17500	F3?	R2	3.19
	2.900	5.900	406	408	0.900	1.900	17500	F3	R2	3.19
	5.900	7.714	408	410	1.900	1.714	17500	F3	R3	3.19
	7.714	8.300	410	412	1.714	0.300	17400	F3	R3	2.89
	8.300	8.562	412	412	0.300	0.562	17400	F3	R3	2.89
	8.562	9.073	412	412	0.562	1.073	19100	F3?	R3	1.61
	9.073	9.481	412	412	1.073	1.481	18200	F3?	R3	0.20
176-5	9.481	9.889	412	412	1.481	1.889	16700	R3	R3	-0.32
	9.889	10.481	412	414	1.889	0.481	16100	R3	R3	0.36
	10.481	10.800	414	414	0.481	0.800	15100	R3	R3	2.42
	10.800	14.015	414	418	0.800	0.015	15100	R3	F1	2.42
	14.015	14.700	418	418	0.015	0.700	14800	R3	F1	1.81
	14.700	14.807	418	418	0.700	0.807	14800	R5	R5	1.81
	14.807	15.500	418	418	0.807	1.500	15600	R5	R5	3.23
	15.500	15.551	418	418	1.500	1.551	15600	F1	R3	3.23
	15.551	21.718	418	424	1.551	1.701	15100	F1	R3	2.70
	21.718	21.800	424	424	1.701	1.783	17100	F1	R3	3.17
	21.718	22.125	424	426	1.701	0.104	17100	F1?	R3	3.17
	22.125	22.336	426	426	0.104	0.313	16000	F1?	R3	2.73
	22.400	23.400	426	426	0.400	1.400	15800	R5	R5	2.78
	23.400	25.877	426	428	1.400	1.875	15800	F1	R3	2.78
	25.877	28.600	428	432	1.875	0.559	16800	F1	R3	2.70
	28.600	29.215	432	432	0.559	1.174	16800	F3	F1	2.70
	29.215	31.300	432	432	1.174	3.259	15400	F3	F1	3.96

Table 2.8: AADT and growth rate for the last 10 years for Polk Co.

	Growth (2.51) Section 176-4-1	Growth (3.185) Section 176-4-2	Growth (2.885) Section 176-4-3	Growth (1.614) Section 176-4-4	Growth (0.197) Section 176-4-5	Growth (1.1) Section 175-7-1	Growth (-0.32) Section 176-5-1	Growth (0.362) Section 176-5-2	Growth (2.42) Section 176-5-3	Growth (1.81) Section 176-5-4
Year	**AADT**	**AADT**	**AADT**	**AADT**	**AADT**	**AADT**	**AADT**	**AADT**	**AADT**	**AADT**
1994	16700	17500	17400	19100	18200	7500	16700	16100	15100	14800
1993	16900	17200	18300	19500	18600	7100	16000	15800	16400	15300
1992	16000	15600	16400	16500	16100	7500	16100	15900	14100	13700
1991	14600	15100	15800	15200	15600	7600	15600	15800	14800	14500
1990	13900	14100	14500	16700	16300	7100	15800	16000	15000	14300
1989	13400	13300	13800	15900	15500	6800	16500	16200	14500	13800
1988	14400	13800	14900	16900	16500	6500	16500	16300	14100	14100
1987	14000	13400	14400	16600	16300	6900	16400	16300	13900	13600
1986	14200	13900	14700	16300	18200	7100	16400	14500	12500	12300
1985	13100	13000	13400	15800	17500	6800	16800	15700	12300	12800

	Growth (3.23) Section 176-5-5	Growth (3.17) Section 176-5-6	Growth (2.73) Section 176-5-7	Growth (2.775) Section 176-5-8	Growth (2.70) Section 176-5-9	Growth (3.96) Section 176-5-10	Growth (2.52) Section 177-1-1	Growth (2.504) Section 177-1-2	Growth (3.0) Section 177-1-3	Growth (3.96) Section 177-1-4
Year	AADT	AADT	AADT	AADT	AADT	AADT	AADT	AADT	AADT	AADT
1994	15600	17100	16000	15800	16800	15400	16810	23000	19500	21000
1993	15700	16700	16800	16400	17600	15300	16300	22000	18900	19900
1992	14100	15300	15500	15100	16800	14500	17900	21000	18700	17800
1991	14500	15000	15600	15200	17400	15000	15200	21000	18600	17500
1990	14100	15200	15400	15200	16800	14400	16600	22000	19100	18300
1989	13700	14100	14600	14400	15700	13500	15300	21000	17200	16200
1988	13400	13700	14200	13600	15100	12900	15300	19900	16800	15700
1987	13400	13800	14100	13800	15200	12600	15100	19700	15500	15800
1986	12100	12600	12800	12600	13700	10900	13600	19000	14800	14000
1985	11200	13100	13100	12800	13900	11100	13500	18800	15800	15000

	Growth (2.59) Section 177-1-5	Growth (2.50) Section 177-1-6
Year	**AADT**	**AADT**
1994	18000	18500
1993	17600	17600
1992	17500	17500
1991	17400	17900
1990	18900	17500
1989	16100	16400
1988	15700	16100
1987	15800	14200
1986	13900	14800
1985	15000	15700

Table 2.9: Sections, markers, AADT, and growth rate for San Jacinto Co.

San Jacinto Co. 174										
C.S.	B.M.	E.M.	B. R. M.	E. R. M.	B.R.F.D.	E.R.F.D.	AADT	(NB)	(SB)	Growth rate (%)
177-2	0.000	4.291	444	450	1.366	0.297	19800			2.90
	0.000	4.100	444	450	1.366	0.100	19800	F1	R1	2.90
	4.100	4.291	450	450	0.100	0.291	19800	F1	F1	2.90
	4.291	5.143	450	450	0.297	1.146	18700	F1	F1	2.71
	5.143	5.534	450	450	1.150	1.541	19500	F1	F1	1.84
	5.534	7.400	450	452	1.541	1.400	20000	F1	F1	2.13
	7.400	7.522	452	452	1.400	1.522	20000	F2	F2	2.00
	17.351	17.850	452	454	1.522	0.000	20000	F2	F2	2.00
	17.850	19.850	454	456	0.000	0.000	20000	R1	F2	2.00
	19.850	23.216	456	458	0.000	1.364	20000	R1	F2	1.67

Table 2.10: AADT and growth rate for the last 10 years for San Jacinto Co.

	Growth (2.90) Section 177-2-1	Growth (2.71) Section 177-2-2	Growth (1.84) Section 177-2-3	Growth (2.13) Section 177-2-4	Growth (2.0) Section 177-2-5	Growth (2.0) Section 177-2-5	Growth (1.67) Section 177-2-6
Year	AADT	AADT	AADT	AADT	AADT	AADT	AADT
1994	19800	18700	19500	20000	20000	7500	20000
1993	18600	17500	18300	18600	19000	7100	20000
1992	18700	17400	17600	17900	18700	7500	19800
1991	18200	17100	17900	18700	19200	7600	20000
1990	18000	16900	16400	18800	19200	7100	19700
1989	17100	16100	16100	17800	16700	6800	18800
1988	17100	16100	17000	17500	18100	6500	18400
1987	16100	14600	15800	16100	16800	6900	17100
1986	14700	15000	16400	16500	17000	7100	17900
1985	15600	14500	16400	16200	16600	6800	18000

CHAPTER 3. MODELING CRACKING DISTRESS IN PAVEMENT OVERLAYS

INTRODUCTION

Cracking is one of the primary distresses appearing on pavement surfaces. The severity of cracking may be characterized by examining the mean crack spacing, the crack width, and the crack length. However, questions regarding how cracks develop with time and whether the cracking process will continue indefinitely do not appear to have been analyzed on a reasonable physical basis. Thus, in this chapter we attempt to model the evolution of cracking distress on a pavement surface using the information collected over a 5-year period on seven flexible overlays on rigid sections and on seven flexible overlays on flexible sections.

Several factors contribute to pavement cracking distress. For example, temperature differentials (i.e., thermal cycling) occurring during day and night or over different seasons play an important role in pavement cracking. The spring thaw season can generate cracks on a newly built pavement by stressing the subbase or the base of the pavement, while the winter season can accelerate cracking on flexible pavements by rendering the asphalt material brittle. Another factor contributing to cracking distress is high traffic loading. Both factors can induce high tensile stress within some parts of the pavement and initiate cracks. Once a crack is initiated, its growth depends on the external stress conditions, on the material properties of the pavement structure, and on the geometry of the crack — which is to say, the exact propagation of a crack, which need not be unstable, is complex.

Reflective cracks, again generated by external loading and by thermal cycling, initiate at the interface of the overlay and the overlaid pavement. For an asphalt mixture overlay, small cracks may repair themselves as they approach the surface of the overlay; high ambient temperatures can also close surface cracks having small widths. In terms of external loading, it can take thousands or millions of traffic loadings before a crack appears on the overlay's surface.

In view of the complexity of the cracking process, it is fair to ask: Can we in fact model cracking distress using a few pertinent physical variables? In the following, we make this attempt by first modeling the evolution of the total number of cracks using a phenomenological approach; we then address the characteristic number of loadings, N_0, that force a reflection crack toward the surface of an overlay. In this modeling effort, we found that the cumulative number of cracks in each test section follows a logistic curve. This confirms our hypothesis that on a new, properly constructed flexible overlay, the cracking rate should exhibit a lag phase in response to traffic loading (owing to the flexible characteristics of the asphalt cement); furthermore, the number of cracks appearing on a surface cannot continue to grow indefinitely, since the presence of a crack depends on the presence of other cracks in its vicinity. However, there may exist a second phase, or fatigue phase, of overlay deterioration, during which additional severe cracks, pot holes, and alligator cracks develop on the overlay. This second stage of deterioration may not occur on highways if a proper maintenance program is in operation.

The distress maps were delineated for seven condition surveys undertaken as part of Project 987. In 1992, seven flexible overlay sections on rigid pavements and seven flexible overlay sections on flexible pavements were constructed and opened for traffic for future rehabilitation purposes (Allison and McCullough 1994, Cho et al. 1995). According to the condition surveys taken at seven different times, the number of cracks appearing on the surface of the test sections were few but increased sharply about 2 years after the initial construction; thereafter, the number of cracks grew slowly. (See Chapter 1 for detailed descriptions of the sections' structure.)

COUNTING THE NUMBERS OF CRACKS

The cracking pattern on a surface resembles a planar network; that is, it resembles a graph that can be drawn in a plane such that two edges intersect only at a vertex (Chartrand 1977), as illustrated in Figure 3.1. An edge is a straight line segment joining two vertices; it is often referred to as a *bond* in the literature. Defining a *face* as an empty area surrounded by edges and denoting the number of faces, the number of edges, and the number of vertices in a planar graph, as F, E, and V, respectively, one can show that the quantity $\chi = V + F - E = 1$ is a topological invariant, called the Euler number, χ. If a planar graph remains a planar graph, removing an edge has one of the following two consequences: (1) it destroys an edge and a vertex if the edge is a dangling one; and (2) it destroys an edge and reduces the number of faces by 1. In either case, the Euler number, χ, does not change. By repeating this process, one eventually reduces a planar graph down to a single vertex, which is 1. The Euler number, χ, is referred to as a topological invariant because it does not change as a surface distorts by continuous transformation but, rather, depends on the topological properties of the surface.

The number of the edges mentioned above is not the number of cracks on a pavement surface. On a pavement surface, a dangling edge does not have a vertex. It can be shown that the number of cracks conforms to $E - V^*$, where V^* is number of vertices excluding those attached to the dangling edges in a planar graph. Note that this number is invariant for a given configuration of a planar graph; that is, it does not depend on the time sequence of the development of longitudinal and transverse cracks (Liu et al. 1996). For example, in Figure 3.1, assuming that the two longitudinal cracks occur first, then the transverse cracks have six broken pieces, with the total number of cracks totaling eight; or, assuming the process proceeds according to the order of T1, L1, L2, and T2 (see Figure 3.1), then T1 is counted as one crack, L1 as two cracks, L2 as two cracks, and T2 as three cracks, with the number of cracks still totaling eight. For the planar graph in Figure 3.1, there are a total of twelve edges, E, and four vertices, V*; the number E-V* is eight.

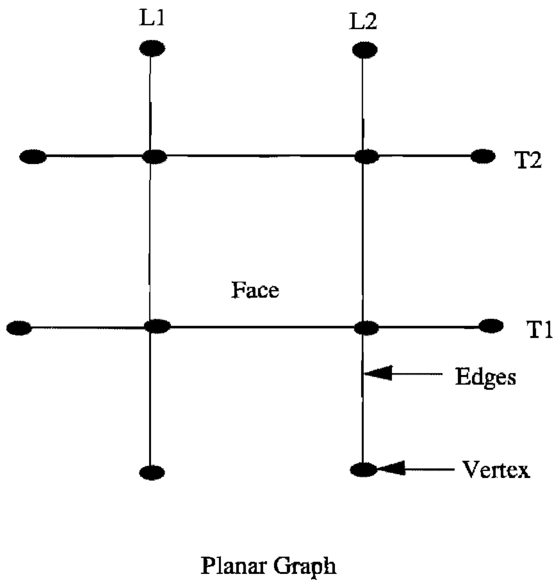

Figure 3.1: A planar graph network.

THE LOGISTIC MODELS FOR CRACKS

For a given section of a roadway, the number of cracks evolves with time. Since the presence of a crack on a pavement surface depends on the existing pattern of cracks, we may model the rate of cracking as

$$dn / dt = f(n) \tag{3.1}$$

Note that, in general, the distress state function *f(n)* can be expanded in terms of a polynomial, namely, $f(n) = a_0 + a_1 n + a_2 n^2 + \text{hot}$, where "hot" means higher-order terms. Since the rate of cracking is low initially, we have $a_0 \sim 0$. Because the cracking rate does not increase indefinitely with time, the third term $a_2 n^2$ with a_2 negative should be retained. Why are other higher-order terms discarded? By introducing more terms up to powers m>2, in general, one creates m–1 peaks for the rate of cracking. However, there is no evidence showing the existence of multiple peaks in the rate of cracking. Thus, we take $f(n) = a_1 n + a_2 n^2$, i.e., $f(n) = \lambda n(n_s - n)$. Equation (3.1) now becomes the well-known Verhulst (logistic) differential equation (Montroll and Badger 1974):

$$dn / dt = \lambda n(n_s - n) \tag{3.2}$$

where *n* is the number of cracks at time *t*, n_s is the saturation value for *n*, and λ is the parameter for the rate of cracking. Setting $y = n / n_s$, Eq. (3.2) can be rewritten as

$$dy / dt = \lambda n_s y(1 - y), \tag{3.3}$$

yielding

$$y = 1 / \left[1 + \exp(-\lambda n_s (t - t_0))\right] \tag{3.4}$$

where t_0, λ, and n_s are determined using the available survey information. The right-hand side of Eq. (3.2) can be written as $-\lambda(n - n_s / 2)^2 + \lambda n_s^2 / 4$. This implies that the maximum rate of cracking is $\lambda n_s^2 / 4$ at $n = n_s / 2$, corresponding to $y = 1/2$. Differentiating the *rhs* of Eq. (3.2) once, one finds that $d^2 n / dt^2 = -\lambda(2n - n_s) dn / dt$, i.e., the second derivative of *n* changes its sign at the maximum rate of cracking. Hence, t_0 is the inflection point of the logistic curve and the time when the rate of cracking rate is at its maximum value $\lambda n_s^2 / 4$. A time interval segment around the inflection point can be defined to indicate the time scale of the cracking process. The time Δt that it takes a crack pattern on an overlay to evolve from a fraction of cracks y_1 to a fraction of cracks y_2 is $(1 / b)\ln[y_2(1 - y_1) / y_1(1 - y_2)]$, yielding $\Delta t = (2 / b)\ln[(1 + 2\delta) / (1 - 2\delta)]$ for $y_1 = 0.5 - \delta$ and $y_2 = 0.5 + \delta$, respectively. For example, using $\delta = 0.4$ for a range from 10% to 90%, one finds that $\Delta t = b^{-1} \ln 81$. Denoting $x = \ln[(1 - y) / y]$, we can write

$$x = \lambda n_s t_0 - \lambda n_s t = a - b\, t, \tag{3.5}$$

where $a = \lambda n_s t_0$, and $b = \lambda n_s$. The parameters in Eq. (3.5) can be found by a regression analysis of the existing data.

By counting the number of cracks from the distress maps recorded in eight condition surveys for Project 987, we obtained the cumulative number of cracks at different times of the surveys. The data for the rigid sections are then analyzed using the logistic model with the first six data points; the corresponding logistic curves and the data points are plotted in Figure 3.2, while Table 3.2 shows the number of cracks appearing in the overlays. Note that the crack number found in the last condition survey is not plotted in the figure, so one may see that the prediction of the logistic curve for the cumulative crack number no longer holds beyond the 5.4-year condition survey period for all the rigid sections. All the numerical values for the parameters $a = \lambda n_s t_0$, and $b = \lambda n_s$, for each section are also listed. The Δt for a range from 10% to 90% for sections R0 – R6 are found to be 2.4, 2.1, 2.5, 3.2, 3.2, 3.0, and 1.7 years, respectively. The times t_0 associated with the maximum rate of cracking for rigid sections R0 – R6 are approximately 1.9, 1.4, 1.9, 2.2, 2.7, 2.6, and 1.5 years, respectively.

Table 3.1: Number of cracks appearing on overlays on rigid sections.

Tm (yr)	R1	R2	R3	R4	R5	R6	R0	MESAL (millions of ESALs)
0.667	44	15	0	1	3	31	17	0.189
1.083	95	39	2	3	7	33	30	0.307
1.500	106	43	8	6	8	35	33	0.425
1.750	205	85	8	12	37	70	66	0.495
2.417	219	106	10	18	45	76	114	0.684
2.917	250	141	19	24	60	92	127	0.826
3.583	250	141	19	24	60	92	127	1.014
4.083	256	215	21	27	61	98	129	1.156
4.583	287	321	21	33	75	105	151	1.298
5.417	329	369	93	83	111	132	?	1.534

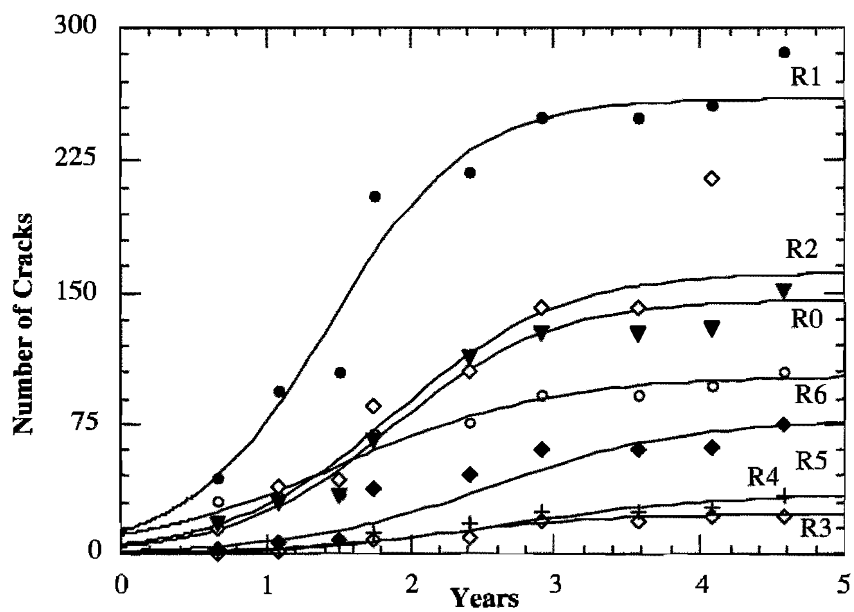

R0: R^2=0.966, $_s$=146, a=3.45,
R1: R^2=0.944, $_s$=260, a=2.93,
R2: R^2=0.963, $_s$=162, a=3.31,
R3: R^2=0.865, $_s$=23, a=3.88,
R4: R^2=0.930, $_s$=35, a=3.73,
R5: R^2=0.900, $_s$=78, a=3.76,
R6: R^2=0.891, $_s$=103, a=2.10,

Figure 3.2: Logistic modeling of cracks in overlays on rigid sections.

Among the seven flexible sections, no analysis was performed for sections F5 and F6 owing to insufficient data. Section F6 has only one real data point; the rest are zeroes. Section F5 basically is a very poor section, one having long stretches of patches and alligator cracks. The logistic curves for sections F0–F4 are plotted in Figure 3.3 along with the observational data. The Δt for a range from 10% to 90% for flexible sections F0–F4 are 2.4, 1.4, 6.9, 2.1, and 1.5 years, respectively. The times t_0 associated with the maximum rate of cracking for rigid sections F0–F4 are approximately 2.8, 3.1, 4.9, 3.1, and 2.7 years, respectively.

The rigid and flexible test sections were opened to traffic in April 1992 and June 1992, respectively. The parameters a and b for both the overlays on rigid pavements and those over flexible pavements are listed in Figures 3.2 and 3.3, respectively. The logistic predictions for the cumulative number of cracks are denoted by the solid lines, while the observational data points are represented by various symbols. Note that the cumulative crack number for the last condition survey is not plotted in Figure 3.3; consequently, one sees that the development of cracks follows a logistic curve not more than 5.2 years for the flexible sections, with the exceptions of F5 and F6. One finds in general that the maximum rate of cracking for an overlay occurs at approximately 2 years after construction for overlays on rigid pavements, and 3 years for those on flexible pavements. It is apparent that the maximum rate of cracking for most of the sections occurs during the winter/spring season. Moreover, on average, the maximum rates of cracking for overlays on rigid pavements take place approximately one year earlier than takes place for overlays on flexible pavement. This may be explained physically by noting that the overlays on rigid pavements suffer stress levels relatively higher than those found on flexible pavements.

Table 3.2: Number of cracks appearing on overlays on flexible sections.

Tm (yr)	F0	F1	F2	F3	F4	F6	MESAL
0.417	1	1	1	0	0	0	0.118
0.833	2	3	1	0	2	0	0.236
1.250	2	3	1	0	2	0	0.354
1.500	3	8	3	2	3	0	0.425
2.167	22	16	3	6	13	0	0.614
2.667	60	30	3	20	92	1	0.755
3.417	66	30	3	23	104	2	0.967
3.833	74	52	6	34	117	3	1.085
4.333	85	58	8	41	124	6	1.227
5.167	90	96	29	127	200	12	1.463

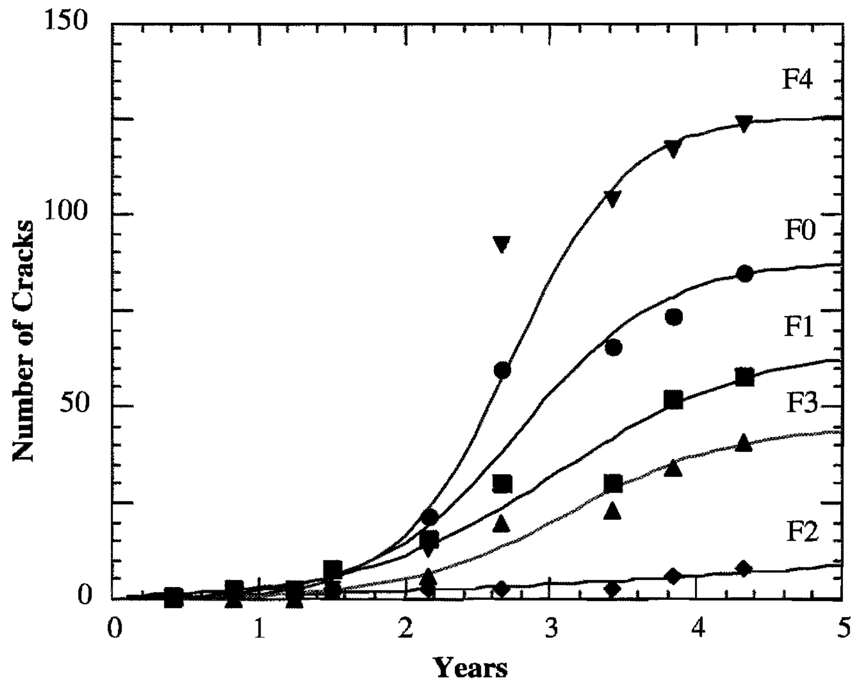

F0: n_s=88, R^2=0.963, a=5.69,
F1: n_s=66, R^2=0.968, a=4.52,
F2: n_s=17, R^2=0.850, a=3.12,
F3: n_s=45, R^2=0.971, a=5.68,
F4: n_s=126, ^{2}=0.962, a=6.95,

Figure 3.3: Logistic modeling of cracks in overlays on flexible sections.

Next we try to correlate the equivalent single axle loads (ESALs) associated with the maximum rate of cracking for an overlay having thickness *h* of the overlay on a pavement. Following the phenomenological approach initiated by Paris and Erdogan (1961), we write

$$d\ell / dN = c\, \ell^{m} \tag{3.6}$$

where ℓ is the length of a crack in the direction consistent with the interface between an overlay and the underlying structure. The parameters *c* and *m* are associated with the material and structural properties of the pavements. The quantities *c* and *m* can be estimated if more than two data points are available. If the moving-upward process of cracking does not depend strongly on the initial size of a crack, the parameter *m* will be in the range of $m < 1$. Solving Eq. (3.5) and assuming the initial size of a crack, ℓ_0, is small, namely, $\ell_0 / h << 1$, we find that

$$N_0 \propto h^{1-m} \tag{3.7}$$

This implies that if the pavement thickness were increased to h_1, then the number of ESALs, N_1, associated with the maximum rate of cracking would be increased to $N_1 = N_0(h_1/h)^{1-m}$. However, there are no test sections having the same underlying structures that are paved with different thicknesses of overlays using the same materials. The best one can do is to pair R2A and R2B, and F0A and F0B, respectively. The analysis for the R2A and R2B pair indicates that *m* is slightly larger than 1. This implies that increasing the thickness of an overlay may not be an effective way to retard reflective cracking. The section F0B shows only two cracks for the 4-year period; hence, no analysis can be performed for the F0A and F0B pair.

GENERAL FORMULATION FOR THE RATE OF CRACKING

The difficulty in Figure 3.2 is explaining the presence of initial cracks in the overlay surfaces; that is, how can one expect cracks to appear immediately on the pavement surface at time $t = 0$ right after the construction? This appears to be a problem for several rigid overlays using a logistic approach and assuming the initial rate of cracking is low. The problem can be solved by adding the initial rate of cracking, which is monotonically decreasing with time, to the right-hand side of Eq. (3.2).

In general, the rate of cracking can be modeled by the following equation:

$$dn/dt = \lambda n(n_s - n) + \chi_0(t) + \chi_s(t) \tag{3.8}$$

where $\chi_0(t)$, which characterizes the initial cracking rate when the pavement is weak, is a monotonic decreasing function of time. Function $\chi_s(t)$, which characterizes the sudden cracking of a pavement owing to some unexpected event, is a stochastic function of time. The functional form of $\chi_s(t)$ may be taken as $\sum_k n_k \delta(t - t_k)$, where n_k is the number of cracks created in a short time as a result of an unexpected event that occurs at time t_k. Note that Eq. (3.8) can be very complex if, in addition, the saturation value n_s is time dependent.

Consider a roadway that suffers no unexpected external impacts after it is opened for traffic: One can then simplify Eq. (3.8) as

$$dn/dt = \lambda n(n_s - n) + \chi_0(t) + n_0\delta(t) \tag{3.9}$$

where n_0 is the initial number of cracks of a new overlay, or a rigid pavement in its "embryo" stage. There are two cases to be considered here, namely, $n_0 = 0$ and $n_0 \neq 0$. However, the rate equation for the latter case can be transformed to that of the former case. Denoting $n = \bar{n} + n_0$, one can write the rate equation for $n_0 \neq 0$ as

$d\bar{n}/dt = \lambda\bar{n}(\bar{n}_s - \bar{n}) + \bar{\chi}_0(t)$, where $\bar{n}_s = n_s - 2n_0$, and $\bar{\chi}_0(t) = \chi_0(t) + \lambda n_0(n_s - n_0)$. In view of the above discussion, one can solve Eq. (3.9) in general by taking $n_0 = 0$, so that

$$dn/dt = \lambda n(n_s - n) + \chi_0(t) \tag{3.10}$$

Setting $n(t) = (\lambda u)^{-1} du/dt$, we transform Eq. (3.10) to the following form:

$$d^2u/dt^2 - b\,du/dt - \lambda\chi_0(t)\,u = 0 \tag{3.11}$$

where $b = \lambda n_s$. Equation (3.11) is a linear second-order differential equation. Employing $u = z\exp(bt/2)$, we obtain a simpler form of Eq. (3.11):

$$d^2z/dt^2 - [\frac{b^2}{4} + \lambda\chi_0(t)]\,z = 0 \tag{3.12}$$

Initial Parabolic Rate of Cracking

The solution of Eq. (3.12) depends on the functional form of $\chi_0(t)$, which may be chosen as

$$\chi_0(t) = \begin{cases} \beta_0(t - t_0)^2 & t \le t_0 \\ 0 & t > t_0 \end{cases} \tag{3.13}$$

where both β_0 and t_0 are parameters. Note that if Eq. (3.13) is employed, Eq. (3.12) becomes the transformed logistic equation for time $t > t_0$ and a Hermite or Weber type differential equation for time $t \le t_0$, namely,

$$d^2z/dt^2 - [b^2/4 + \lambda\beta_0(t - t_0)^2]\,z = 0 \tag{3.14}$$

Making the transformation $z = w\exp[-\beta\tau^2/2]$, we rewrite Eq. (3.14) as

$$d^2w/d\tau^2 - 2\beta\,\tau\,dw/d\tau - [\frac{b^2}{4} + \beta]\,w = 0 \tag{3.15}$$

where $\beta^2 = \lambda\beta_0$. Both β and b^2 have the same dimension, s^{-2}. Eq. (3.15), a nonsingular differential equation, can be solved by using a power series method. Setting $w(\tau) = \sum_{k=0}^{\infty} a_k \tau^k$, we obtain

$$a_{j+2} = (2\beta j + \gamma)\,[(j+2)(j+1)]^{-1} a_j \tag{3.16}$$

where $\gamma = \beta + \frac{b^2}{4}$, yielding the two series solutions as

$$\begin{aligned} w_1(\tau) &= 1 + \sum_{j=1}^{\infty} \frac{[(4n-4)\beta+\gamma]\,[(4n-8)\beta+\gamma]\cdots\gamma}{(2n)!} a_{2n}\tau^{2n} \\ w_2(\tau) &= \sum_{j=1}^{\infty} \frac{[(4n-2)\beta+\gamma]\,[(4n-6)\beta+\gamma]\cdots[2\beta+\gamma]}{(2n+1)!} a_{2n+1}\tau^{2n+1} \end{aligned} \tag{3.17}$$

Equation (3.16) implies that $a_{j+2}/a_j \to 0$ when $j \to \infty$. Thus, both $w_1(\tau)$ and $w_2(\tau)$ converge for arbitrary values of τ. Moreover, it can be shown that both $dw_1/d\tau$ and $dw_2/d\tau$ converge for any value of τ. The general solution of Eq. (3.15) is the linear combination of functions $w_1(\tau)$ and $w_2(\tau)$, i.e., $w(\tau) = c_1 w_1(\tau) + c_2 w_2(\tau)$. Thus, the solution $n(t)$ of Eq. (3.10) for $t \le t_0$ can be written as

$$n(t) = \lambda^{-1}\left(\frac{b}{2} - \beta\tau + \frac{1}{w}\frac{dw}{d\tau}\right) \tag{3.18}$$

Note that n(t) depends only on the ratio of the coefficients c_1 and c_2. Using the boundary condition n(0)=0 we obtain

$$\frac{c_1}{c_2} = -\frac{(\beta t_0 + b/2) w_2(-t_0) + w_2'(-t_0)}{(\beta t_0 + b/2) w_1(-t_0) + w_1'(-t_0)} \tag{3.19}$$

For convenience, we choose $c_1 = (\beta t_0 + b/2) w_2(-t_0) + w_2'(-t_0)$ and $c_2 = (\beta t_0 + b/2) w_1(-t_0) + w_1'(-t_0)$. The solution for Eq. (3.10) then becomes

$$n(t) = \begin{cases} \lambda^{-1}\left(\dfrac{b}{2} - \beta\,\tau + \dfrac{1}{w}\dfrac{dw}{d\tau}\right), & t \le t_0 \\ n_s\eta/(1+\eta)\,, & t > t_0 \end{cases} \tag{3.20}$$

where $\eta = \exp[b(t - t_0)]\, n(t_0) / [n_s - n(t_0)]$. Note that the curve for the number of cracks, $n(t)$, is smoothly joined at time t_0, since the first derivative of $n(t)$ is continuous at t_0. In general, it can be shown that both $n(t)$ and its derivative are continuous at t_0 so long as $\chi_0(t_0)$ vanishes.

We now apply Eq. (3.20) to describe the evolution of cracks on the rigid overlays. Using $t_0 = 0.5$ and $\beta_0 t_0 \sim \sqrt{3\lambda n(t_0)/t_0}$, we obtain the number of cracks $n(t)$ for rigid sections R0, R1, R2, and R6. The analytical results are plotted as solid curves in Figure 3.4, where all the analytic prediction curves go through the origin. The solid circles, the empty circles, the solid diamonds, and the plus signs represent the data collected for sections R0, R1, R2, and R6. For the rest of the rigid sections, the initial rates of cracking are indeed low. We again apply Eq. (3.20) to estimate the number of cracks $n(t)$ and plot the theoretical results as solid curves in Figure 3.5.

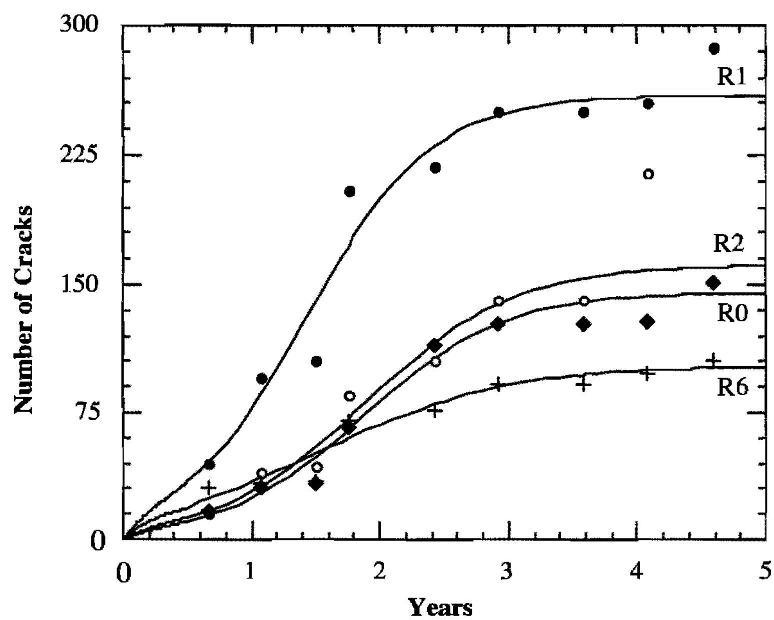

R0: R^2=0.966, $_s$=146, a=3.45, R2: R^2=0.963, $_s$=162, a=3.31,
R1: R^2=0.944, $_s$=260, a=2.93, R6: R^2=0.891, $_s$=103, a=2.10,

Figure 3.4: Evolution of cracks in overlays on R0, R1, R2, and R6 sections considering the initial rate of cracking.

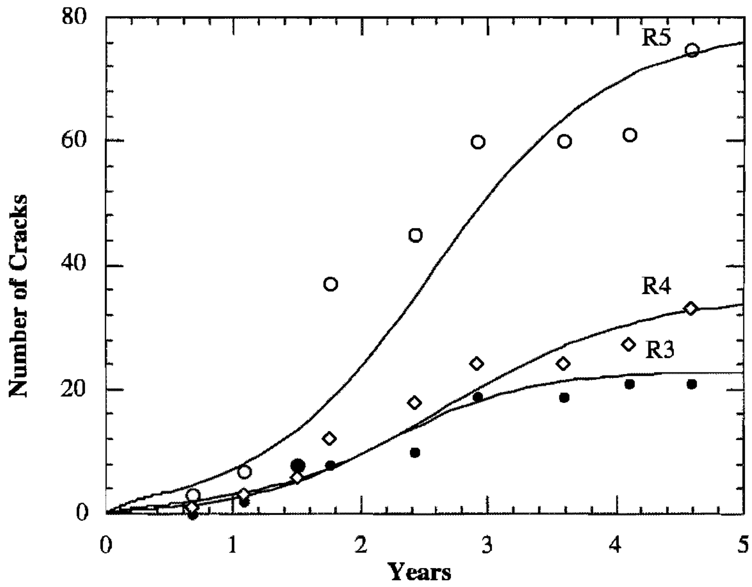

R3 R^2=0.865, $_s$=23, a=3.88, R5 R^2=0.900, $_s$=78, a=3.76,
R4 R^2=0.930, $_s$=35, a=3.73,

Figure 3.5: Evolution of cracks in overlays on R3, R4, and R5 sections considering the initial rate of cracking.

One may now put the curves for all the rigid sections in one single plot and compare them with the results obtained using the simple logistic curves shown in Figure 3.6.

THE AREA OF FATIGUE CRACKING ON OVERLAY SURFACE

Fatigue cracking is another type of pavement surface distress appearing on flexible overlays in some test sections. The severity of fatigue cracking appearing on a pavement surface is usually characterized by the area of cracking. Most of the test sections show little fatigue cracking, with the exceptions of sections F5, R1, and R2. The areas of fatigue cracking for the flexible and rigid sections are estimated using the maps generated from the last eight condition surveys; these sections are shown in Table 3.3 and Table 3.4.

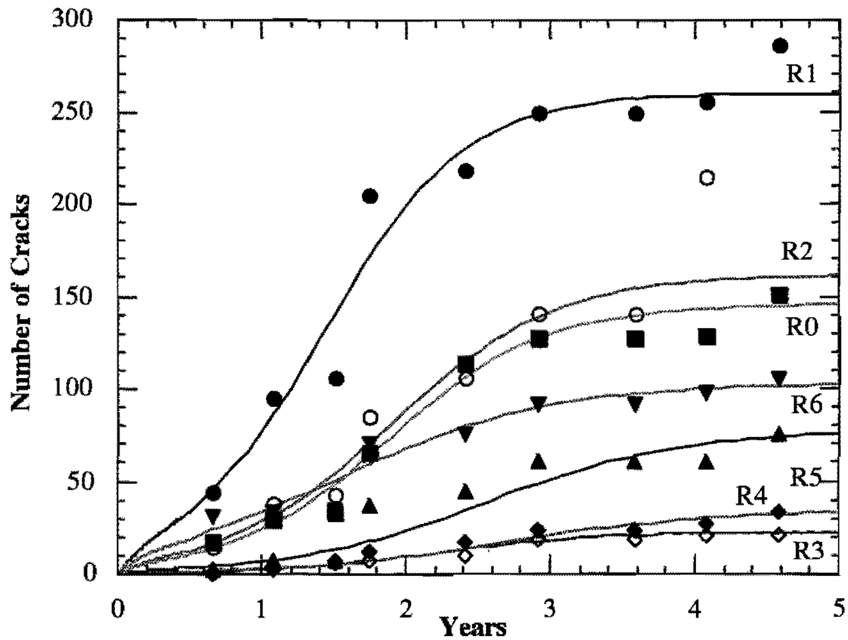

R0: R^2=0.966, $_s$=146, a=3.45,
R1: R^2=0.944, $_s$=260, a=2.93,
R2: R^2=0.963, $_s$=162, a=3.31,
R3: R^2=0.865, $_s$=23, a=3.88,
R4: R^2=0.930, $_s$=35, a=3.73,
R5: R^2=0.900, $_s$=78, a=3.76,
R6: R^2=0.891, $_s$=103, a=2.10,

Figure 3.6: Evolution of cracks in overlays on rigid sections considering the initial rate of cracking.

Table 3.3: Area of fatigue cracking in overlays on rigid pavement.

Time	R0	R1	R2	R3	R4	R5	R6
Dec-92	0	25	0	0	0	0	24
May-93	0	49	149	0	60	70	24
Oct-93	0	52	149	48	120	290	44
Jan-94	24	177	359	60	120	306	64
Mar-95	24	189	805	338	154	310	74
Nov-95	81	566	1355	338	320	325	81
May-96	85	761	4425	338	700	325	99
Nov-96	113	890	5556	338	700	415	181
Sep-97	?	916	5556	338	?	?	?

Table 3.4: Area of fatigue cracking in overlays on flexible pavement.

Time	F0	F1	F2	F3	F4	F5	F6
Dec-92	0	0	0	0	0	0	0
May-93	0	0	0	0	0	0	0
Oct-93	80	0	0	30	0	767	400
Jan-94	179	0	10	30	0	3267	400
Mar-95	227	0	10	30	120	4242	400
Nov-95	257	12	10	108	227	4242	400
May-96	287	84	10	147	248	4242	400
Nov-96	287	84	18	147	263	4242	412
Sep-97	297	84	28	168	299	6000	460

It is known that the area of fatigue cannot go on indefinitely, since the worst-case scenario is one where the surface is filled with fatigue cracks. Using the boundary condition that $n_s = 1$, corresponding to a situation in which the entire surface is saturated with fatigue cracks, one can proceed to solve Eq. (3.2) to express the evolution of the cracking area S in terms of the MESAL y. The results derived for the flexible test sections are given by:

$$\begin{aligned}
&\text{F0:} \quad S = [1+\exp(5.38-0.96y)]^{-1}; \quad R^2 = 0.69 \\
&\text{F1:} \quad S = [1+\exp(9.65-3.10y)]^{-1}; \quad R^2 = 0.51 \\
&\text{F2:} \quad S = [1+\exp(8.27-0.96y)]^{-1}; \quad R^2 = 0.63 \\
&\text{F3:} \quad S = [1+\exp(7.29-1.88y)]^{-1}; \quad R^2 = 0.84 \\
&\text{F4:} \quad S = [1+\exp(5.77-1.17y)]^{-1}; \quad R^2 = 0.77 \\
&\text{F5:} \quad S = [1+\exp(2.85-1.44y)]^{-1}; \quad R^2 = 0.59 \\
&\text{F6:} \quad S = [1+\exp(3.95-0.09y)]^{-1}; \quad R^2 = 0.50
\end{aligned} \tag{3.21}$$

and the results for the rigid sections are

$$
\begin{array}{lll}
\text{R0:} & S=\left[1+\exp(8.00-2.18y)\right]^{-1}; & R^2=0.82 \\
\text{R1:} & S=\left[1+\exp(7.03-3.22y)\right]^{-1}; & R^2=0.94 \\
\text{R2:} & S=\left[1+\exp(6.33-4.07y)\right]^{-1}; & R^2=0.96 \\
\text{R3:} & S=\left[1+\exp(6.80-2.44y)\right]^{-1}; & R^2=0.81 \\
\text{R4:} & S=\left[1+\exp(6.40-2.40y)\right]^{-1}; & R^2=0.92 \\
\text{R5:} & S=\left[1+\exp(5.14-1.03y)\right]^{-1}; & R^2=0.45 \\
\text{R6:} & S=\left[1+\exp(6.87-1.53y)\right]^{-1}; & R^2=0.85
\end{array}
\tag{3.22}
$$

The logistic model appears to provide a good description of the development of fatigue cracking areas appearing in overlays on both flexible and rigid pavements. One can estimate easily the failure MESAL loading y associated with certain criteria of pavement failure for fatigue cracking. Assuming S_{fail} is the criterion of fatigue cracking failure in a pavement surface, one can find that the loading y associated with the criterion for a section is given by

$$y_{fail} = \left\{a - \ln\left[(1 - S_{fail}) / S_{fail}\right]\right\} / b \tag{3.23}$$

For example, assuming $S_{fail} = 10\%$, for section R0, a=8.00, and b=2.18, y_{fail} is found to be 2.66 MESAL, corresponding to approximately 9 year's of traffic loading.

The logistic model is presented for the development of fatigue cracks. One may apply a linear model

$$S = ay + b \tag{3.24}$$

to the existing data in Table 3.3 and Table 3.4 — so long as fatigue cracking has not become severe within the overlays; a and b are the regression coefficients that can be derived easily from the data, and y is a million ESALs.

CHAPTER 4. RUTTING DEVELOPMENT IN PAVEMENT OVERLAYS

Another important pavement distress is the rut depth developed over a period of time along the wheelpaths on a pavement surface. It is known that the key factor contributing to rut depth, namely, the permanent deformation appearing in the pavement surface, comes from all the layers of a flexible pavement or solely from the surface layer for the overlays on rigid pavement. The surface rut depth for flexible pavement is believed to be mainly due to the deformation of the pavement along the subgrade (Finn and Monismith 1984, Monismith 1992). The primary factor contributing to rutting in the test sections is traffic loading. There are other effects, such as shear failure, creep effects, and other types of subbase movement, that can contribute to rutting. Plastic flow (i.e., shear failure) is observed in some portions of sections F5 and F0. The creep effect should not be of any significance in the test sections, since no long-term static loads (excluding the dead load of the pavement structure) have been applied to the surfaces of the test sections.

The rut depth data for the test sections have been collected eight times for both traffic lanes in the test sections over the last 4 years. The rut depth is measured using a 1.8-m (6-ft) straight bar for every 15.25-m (50-ft) spacing along each wheel track of the test sections. In total, eighty data points have been collected for each survey of a test section. Since the ratio of traffic loading between the right and left lane is approximately 8:1, the data for the right lane (R.L.) and left lane (L.L.) should be handled separately. It was found that the distributions of rut depth data for both lanes follow the Gamma distribution quite well. The results are shown in Table 4.1through Table 4.14; also shown are the rut depth and other parameters for the Gamma distributions of the form $f(r)=\left[b^a\Gamma(a+1)\right]^{-1} r^{a-1}e^{-r/b}$. The average and the variance of the distribution are $\bar{r}=ab$ and $\sigma=ab^2$, respectively.

The rut depth data are presented in the following fourteen tables for each of the test sections. For the first 2-year period of observation, the rut depth data for most of the sections fluctuate. Then, the rut depth evolves to a linear growth period for the rest of the observational period. It is expected that the rut depth will continue to grow at a relatively stable rate for some time (i.e., beyond our monitoring period). In the tables, we use R.L. for the right lane (outside lane) and L.L. for the left lane (inside lane). The number of annual ESALs for the test sections is approximately 0.283 million for both lanes; 88% of it is distributed in the R.L.

Table 4.1: Parameters for Gamma distribution, the theoretical rut depth (RD), the raw rut depth (RRD), and the time (Tm) duration for which section R0 has been exposed to traffic (1 in.=25.4 mm).

R0										
		L. L.						R. L.		
a	b	χ2	RD	RRD	Tm	a	b	χ2	RD	RRD
2.20	0.020	2.92	0.043	0.058	0.50	3.60	0.011	0.77	0.038	0.027
3.00	0.014	2.46	0.042	0.046	0.75	1.45	0.022	1.16	0.032	0.030
2.70	0.009	0.24	0.023	0.020	1.00	1.70	0.016	0.60	0.026	0.035
2.45	0.017	0.89	0.042	0.030	1.50	2.30	0.020	1.10	0.046	0.029
4.65	0.009	0.44	0.040	0.036	1.92	2.90	0.013	0.47	0.038	0.026
1.35	0.029	0.30	0.039	0.055	3.58	2.05	0.023	0.75	0.048	0.057
1.00	0.057	4.70	0.057	0.053	4.08	3.10	0.021	1.10	0.065	0.065

Table 4.2: Parameters for Gamma distribution, the theoretical rut depth (RD), the raw rut depth (RRD), and the time (Tm) duration for which section R1 has been exposed to traffic (1 in.=25.4 mm).

R1										
		L. L.						R. L.		
a	b	χ2	RD	RRD	Tm	a	b	χ2	RD	RRD
1.70	0.017	0.41	0.028	0.027	0.50	4.25	0.010	1.17	0.044	0.042
1.30	0.022	0.71	0.028	0.027	0.75	3.75	0.013	1.02	0.048	0.047
3.60	0.013	1.01	0.047	0.043	1.00	1.60	0.023	1.01	0.037	0.036
1.75	0.019	0.05	0.032	0.034	1.50	1.20	0.023	0.23	0.028	0.033
2.40	0.015	0.94	0.035	0.037	1.92	*	*	*	*	0.042
1.50	0.025	2.39	0.037	0.038	3.58	1.60	0.018	0.21	0.029	0.041
2.75	0.022	2.56	0.059	0.059	4.08	1.95	0.027	0.16	0.052	0.059

Table 4.3: Parameters for Gamma distribution, the theoretical rut depth (RD), the raw rut depth (RRD), and the time (Tm) duration for which section R2 has been exposed to traffic (1 in.=25.4 mm).

R2										
		L. L.						R. L.		
a	b	χ2	RD	RRD	Tm	a	b	χ2	RD	RRD
2.15	0.017	1.73	0.037	0.035	0.50	2.05	0.037	0.48	0.076	0.079
3.25	0.016	2.16	0.053	0.054	0.75	1.85	0.052	0.20	0.096	0.100
2.10	0.039	0.33	0.082	0.088	1.00	2.10	0.036	1.60	0.076	0.079
3.00	0.012	2.00	0.035	0.033	1.50	1.35	0.063	0.24	0.085	0.094
2.05	0.019	0.96	0.038	0.039	1.92	1.16	0.098	0.05	0.114	0.112
2.15	0.020	0.51	0.042	0.043	3.58	2.13	0.072	1.29	0.152	0.148
2.55	0.020	0.87	0.051	0.054	4.08	1.80	0.098	0.18	0.176	0.173

Table 4.4: Parameters for Gamma distribution, the theoretical rut depth (RD), the raw rut depth (RRD), and the time (Tm) duration for which section R3 has been exposed to traffic (1 in.=25.4 mm).

R3										
		L. L.						R. L.		
a	b	χ2	RD	RRD	Tm	a	b	χ2	RD	RRD
2.400	0.023	0.205	0.055	0.055	0.50	1.700	0.134	0.205	0.227	0.211
2.700	0.027	1.620	0.073	0.085	0.75	1.560	0.144	1.620	0.224	0.215
2.350	0.027	1.940	0.063	0.067	1.00	3.000	0.089	1.940	0.267	0.251
2.200	0.027	0.160	0.058	0.050	1.50	2.100	0.063	0.160	0.131	0.127
2.700	0.028	0.460	0.074	0.074	1.92	2.150	0.074	0.460	0.158	0.148
2.100	0.039	0.460	0.081	0.077	3.58	2.750	0.075	0.460	0.205	0.190
2.050	0.052	0.146	0.106	0.102	4.08	2.900	0.067	0.670	0.193	0.195

Table 4.5: Parameters for Gamma distribution, the theoretical rut depth (RD), the raw rut depth (RRD), and the time (Tm) duration for which section R4 has been exposed to traffic (1 in.=25.4 mm).

R4										
		L. L.						R. L.		
a	b	$\chi 2$	RD	RRD	Tm	a	b	$\chi 2$	RD	RRD
1.900	0.035	1.680	0.066	0.063	0.50	2.350	0.024	0.410	0.056	0.052
1.600	0.042	2.000	0.067	0.062	0.75	2.700	0.017	0.190	0.045	0.044
2.000	0.033	0.290	0.066	0.061	1.00	1.950	0.024	1.610	0.047	0.048
1.250	0.035	1.350	0.043	0.044	1.50	3.050	0.019	2.810	0.058	0.057
3.800	0.015	2.820	0.057	0.064	1.92	1.700	0.035	0.740	0.059	0.059
1.500	0.033	2.610	0.049	0.048	3.58	3.200	0.019	2.610	0.061	0.068
2.450	0.027	0.036	0.065	0.064	4.08	3.100	0.025	0.330	0.077	0.081

Table 4.6: Parameters for Gamma distribution, the theoretical rut depth (RD), the raw rut depth (RRD), and the time (Tm) duration for which section R5 has been exposed to traffic (1 in.=25.4 mm).

R5										
		L. L.						R. L.		
a	b	$\chi 2$	RD	RRD	Tm	a	b	$\chi 2$	RD	RRD
2.900	0.018	2.850	0.051	0.050	0.50	3.600	0.013	1.760	0.045	0.045
4.000	0.013	2.630	0.053	0.051	0.75	2.450	0.015	1.140	0.037	0.037
1.375	0.034	0.830	0.047	0.042	1.00	1.300	0.027	0.420	0.035	0.033
4.750	0.011	2.710	0.052	0.051	1.50	2.250	0.026	6.100	0.057	0.053
2.500	0.024	4.000	0.059	0.061	1.92	1.850	0.028	2.890	0.052	0.052
2.300	0.025	0.092	0.058	0.059	3.58	1.500	0.039	3.820	0.059	0.057
1.700	0.037	0.790	0.062	0.059	4.08	2.000	0.034	0.140	0.067	0.065

Table 4.7: Parameters for Gamma distribution, the theoretical rut depth (RD), the raw rut depth (RRD), and the time (Tm) duration for which section R6 has been exposed to traffic (1 in.=25.4 mm).

R6										
		L. L.						R. L.		
a	b	$\chi2$	RD	RRD	Tm	a	b	$\chi2$	RD	RRD
2.400	0.018	6.400	0.043	0.041	0.50	3.150	0.013	1.520	0.039	0.035
4.050	0.013	3.500	0.051	0.040	0.75	1.350	0.025	5.980	0.033	0.029
2.600	0.019	0.230	0.050	0.047	1.00	2.075	0.013	0.770	0.026	0.024
2.500	0.017	0.890	0.042	0.045	1.50	2.550	0.018	1.540	0.045	0.037
3.650	0.011	0.045	0.041	0.040	1.92	2.600	0.016	0.410	0.040	0.039
1.350	0.029	0.300	0.039	0.039	3.58	1.950	0.025	1.030	0.049	0.047
2.250	0.022	0.310	0.048	0.047	4.08	2.800	0.018	2.050	0.050	0.046

Table 4.8: Parameters for Gamma distribution, the theoretical rut depth (RD), the raw rut depth (RRD), and the time (Tm) duration for which section F0 has been exposed to traffic (1 in.=25.4 mm).

F0										
		L. L.						R. L.		
a	b	$\chi2$	RD	RRD	Tm	a	b	$\chi2$	RD	RRD
2.300	0.014	0.750	0.031	0.028	0.00	1.850	0.033	2.720	0.060	0.057
3.350	0.013	0.630	0.044	0.044	0.25	2.150	0.032	6.000	0.068	0.060
3.750	0.011	0.380	0.039	0.037	0.50	1.600	0.045	4.200	0.072	0.064
4.100	0.009	0.260	0.035	0.034	0.75	3.850	0.023	0.410	0.087	0.088
3.850	0.008	3.260	0.031	0.031	1.00	1.650	0.045	1.140	0.074	0.065
1.300	0.022	0.250	0.028	0.026	1.25	1.800	0.044	3.270	0.079	0.074
2.600	0.017	0.210	0.043	0.043	1.67	1.550	0.056	1.500	0.087	0.083
1.950	0.024	2.450	0.046	0.045	3.33	1.650	0.062	3.160	0.101	0.093
2.750	0.025	4.650	0.069	0.067	3.83	1.900	0.058	6.700	0.110	0.101

Table 4.9: Parameters for Gamma distribution, the theoretical rut depth (RD), the raw rut depth (RRD), and the time (Tm) duration for which section F1 has been exposed to traffic (1 in.=25.4 mm).

F1										
		L. L.						R. L.		
a	b	$\chi2$	RD	RRD	Tm	a	b	$\chi2$	RD	RRD
1.2400	0.0165	0.0750	0.0205	0.0191	0.00	1.650	0.029	0.590	0.047	0.044
1.7750	0.0140	6.0000	0.0249	0.0245	0.25	2.300	0.021	2.680	0.047	0.045
3.6500	0.0108	0.7000	0.0392	0.0365	0.50	1.080	0.043	9.200	0.046	0.039
2.7000	0.0105	3.4200	0.0284	0.0283	0.75	1.725	0.025	0.496	0.043	0.042
1.6500	0.0290	1.3800	0.0479	0.0423	1.00	1.700	0.013	2.220	0.022	0.019
1.8500	0.0150	1.0000	0.0278	0.0269	1.25	1.600	0.030	2.880	0.048	0.049
1.4500	0.0165	4.2100	0.0239	0.0227	1.67	2.550	0.019	3.850	0.048	0.045
1.2500	0.0285	1.6100	0.0356	0.0374	3.33	1.950	0.037	0.970	0.071	0.068
1.4000	0.0325	1.5400	0.0455	0.0417	3.83	2.650	0.030	2.560	0.080	0.073

Table 4.10: Parameters for Gamma distribution, the theoretical rut depth (RD), the raw rut depth (RRD), and the time (Tm) duration for which section F2 has been exposed to traffic (1 in.=25.4 mm).

F2										
		L. L.						R. L.		
a	b	$\chi2$	RD	RRD	Tm	a	b	$\chi2$	RD	RRD
1.400	0.021	0.560	0.029	0.027	0.00	3.500	0.012	0.560	0.043	0.039
3.050	0.013	0.019	0.040	0.038	0.25	4.700	0.013	0.019	0.059	0.057
2.550	0.017	0.360	0.043	0.040	0.50	1.950	0.023	0.360	0.044	0.044
2.050	0.021	0.065	0.042	0.040	0.75	2.950	0.015	0.065	0.045	0.044
3.800	0.013	1.590	0.048	0.045	1.00	2.900	0.011	1.590	0.031	0.029
2.050	0.015	3.110	0.031	0.028	1.25	10.650	0.006	3.110	0.065	0.042
1.850	0.022	0.610	0.040	0.038	1.67	2.250	0.025	0.610	0.057	0.055
3.050	0.017	0.031	0.050	0.052	3.33	3.850	0.018	0.031	0.067	0.065
3.850	0.017	0.180	0.064	0.059	3.83	3.850	0.019	0.180	0.071	0.069

Table 4.11: Parameters for Gamma distribution, the theoretical rut depth (RD), the raw rut depth (RRD), and the time (Tm) duration for which section F3 has been exposed to traffic (1 in.=25.4 mm).

F3										
		L. L.						R. L.		
a	b	$\chi2$	RD	RRD	Tm	a	b	$\chi2$	RD	RRD
1.350	0.021	0.037	0.028	0.031	0.00	2.050	0.014	1.500	0.029	0.029
1.550	0.021	2.060	0.032	0.030	0.25	9.400	0.006	0.550	0.054	0.054
2.500	0.014	1.480	0.035	0.034	0.50	2.950	0.012	3.270	0.035	0.032
3.150	0.010	3.950	0.032	0.032	0.75	2.350	0.014	0.470	0.033	0.032
2.250	0.014	3.190	0.030	0.029	1.00	2.400	0.015	0.750	0.036	0.035
1.300	0.018	0.340	0.023	0.022	1.25	3.600	0.009	1.850	0.033	0.035
2.250	0.015	3.970	0.034	0.033	1.67	2.850	0.011	2.370	0.031	0.029
2.900	0.016	0.830	0.046	0.043	3.33	2.700	0.018	0.370	0.047	0.047
7.000	0.008	3.500	0.058	0.055	3.83	3.300	0.016	0.680	0.052	0.058

Table 4.12: Parameters for Gamma distribution, the theoretical rut depth (RD), the raw rut depth (RRD), and the time (Tm) duration for which section F4 has been exposed to traffic (1 in.=25.4 mm).

F4										
		L. L.						R. L.		
a	b	$\chi2$	RD	RRD	Tm	a	b	$\chi2$	RD	RRD
2.250	0.022	1.730	0.050	0.049	0.00	2.300	0.013	1.310	0.029	0.026
1.700	0.034	0.890	0.057	0.053	0.25	8.000	0.008	2.260	0.064	0.060
2.800	0.025	0.460	0.069	0.064	0.50	8.200	0.008	2.010	0.066	0.063
2.450	0.020	0.450	0.049	0.047	0.75	4.150	0.010	3.100	0.042	0.037
4.350	0.012	2.150	0.051	0.047	1.00	3.600	0.009	0.810	0.031	0.030
2.050	0.028	0.740	0.057	0.057	1.25	3.350	0.011	0.980	0.037	0.033
3.150	0.018	0.250	0.055	0.052	1.67	2.700	0.011	0.380	0.030	0.036
2.950	0.021	1.660	0.061	0.061	3.33	4.000	0.016	1.700	0.064	0.076
6.050	0.015	1.470	0.088	0.086	3.83	4.500	0.013	0.750	0.059	0.059

Table 4.13: Parameters for Gamma distribution, the theoretical rut depth (RD), the raw rut depth (RRD), and the time (Tm) duration for which section F5 has been exposed to traffic (1 in.=25.4 mm).

F5										
		L. L.						R. L.		
a	b	χ2	RD	RRD	Tm	a	b	χ2	RD	RRD
3.900	0.011	1.380	0.042	0.043	0.00	2.900	0.017	0.330	0.049	0.046
2.950	0.017	3.300	0.050	0.052	0.25	1.100	0.038	0.650	0.042	0.079
3.550	0.014	2.260	0.051	0.041	0.50	1.150	0.038	3.230	0.043	0.040
4.200	0.015	2.110	0.063	0.039	0.75	3.000	0.031	2.680	0.093	0.096
2.700	0.032	4.370	0.086	0.088	1.00	2.000	0.061	0.635	0.121	0.141
1.800	0.055	0.390	0.098	0.096	1.25	1.500	0.087	0.685	0.131	0.146
2.350	0.050	0.250	0.118	0.117	1.67	1.600	0.080	0.420	0.128	0.148
2.300	0.061	2.640	0.140	0.144	3.33	2.550	0.103	0.610	0.263	0.270
3.000	0.055	0.390	0.165	0.165	3.83	2.120	0.134	0.041	0.284	0.275

Table 4.14: Parameters for Gamma distribution, the theoretical rut depth (RD), the raw rut depth (RRD), and the time (Tm) duration for which section F6 has been exposed to traffic (1 in.=25.4 mm).

F6										
		L. L.						R. L.		
a	b	χ2	RD	RRD	Tm	a	b	χ2	RD	RRD
2.700	0.018	0.880	0.047	0.045	0.00	1.850	0.025	0.510	0.046	0.046
2.350	0.024	2.930	0.055	0.049	0.25	3.500	0.014	0.058	0.050	0.053
3.050	0.015	0.840	0.044	0.046	0.50	2.600	0.021	0.300	0.054	0.061
3.250	0.013	0.120	0.042	0.046	0.75	3.025	0.019	0.085	0.057	0.057
2.800	0.019	1.860	0.052	0.055	1.00	3.050	0.017	1.370	0.051	0.052
4.750	0.010	0.160	0.048	0.053	1.25	3.650	0.015	0.690	0.053	0.049
2.600	0.019	0.730	0.049	0.059	1.67	3.850	0.016	0.505	0.060	0.056
2.350	0.025	1.540	0.058	0.086	3.33	2.600	0.028	1.090	0.073	0.071
4.900	0.014	0.080	0.066	0.076	3.83	4.350	0.015	1.750	0.065	0.069

The average raw rut depth for the R.L. (outside lane) is plotted in Figures 4.1 and 4.2 for rigid and flexible test sections, respectively. It can be inferred from the figures that (1) for the first 2 years following construction of the test sections, the rut depth data do not show any regular trend; (2) the average rut depth at the present time for the flexible sections is less than 2.54 mm (0.1 in.) with the exception of F5, which is out of the range of Figure 4.1; (3) the average rut depth for the rigid sections is less than 2.54 mm (0.1 in.) with the exception of sections R2 and R3; (4) in general, the average rut depth grows linearly as the number of axle loadings increases; it is expected to saturate and plateau in the future; and (5) the sudden drop of the rut depth for all the rigid sections except R5 in the last survey is due to the fact that portions of these sections have been resurfaced.

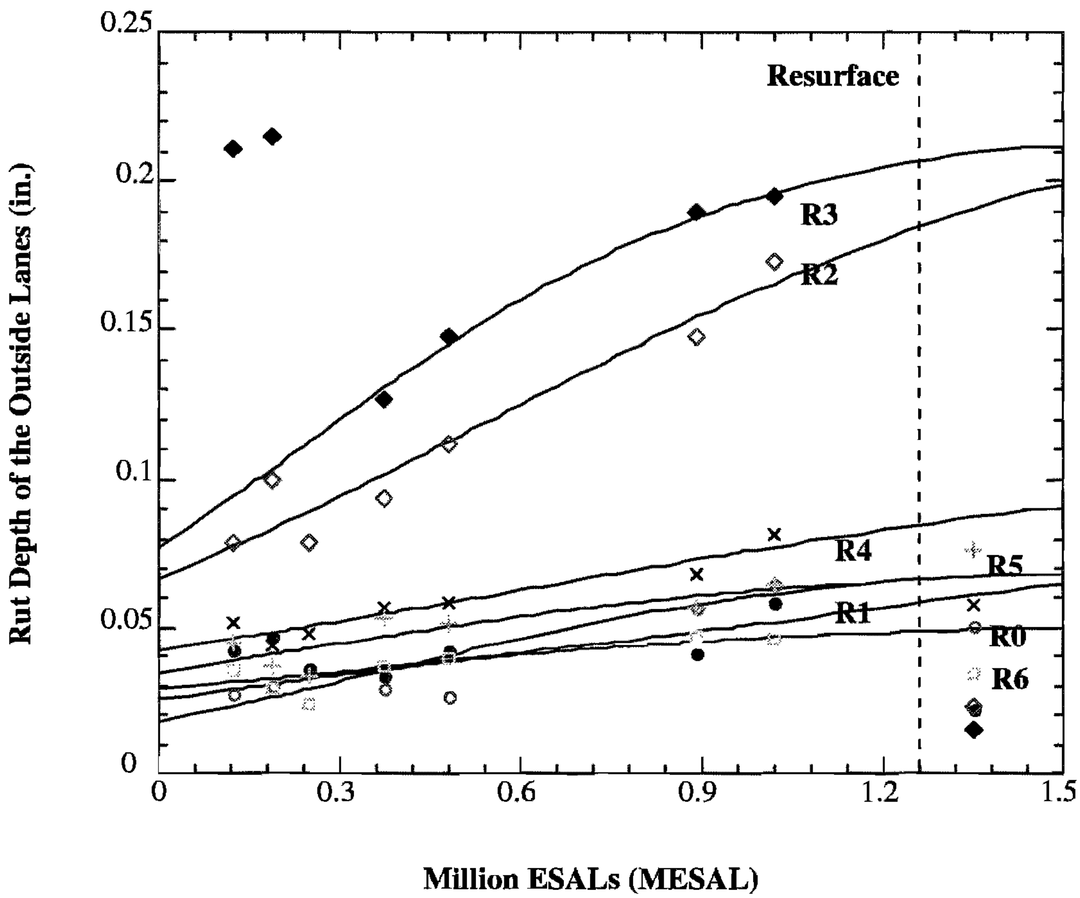

Figure 4.1: Rut depth of the outside lanes of rigid sections.

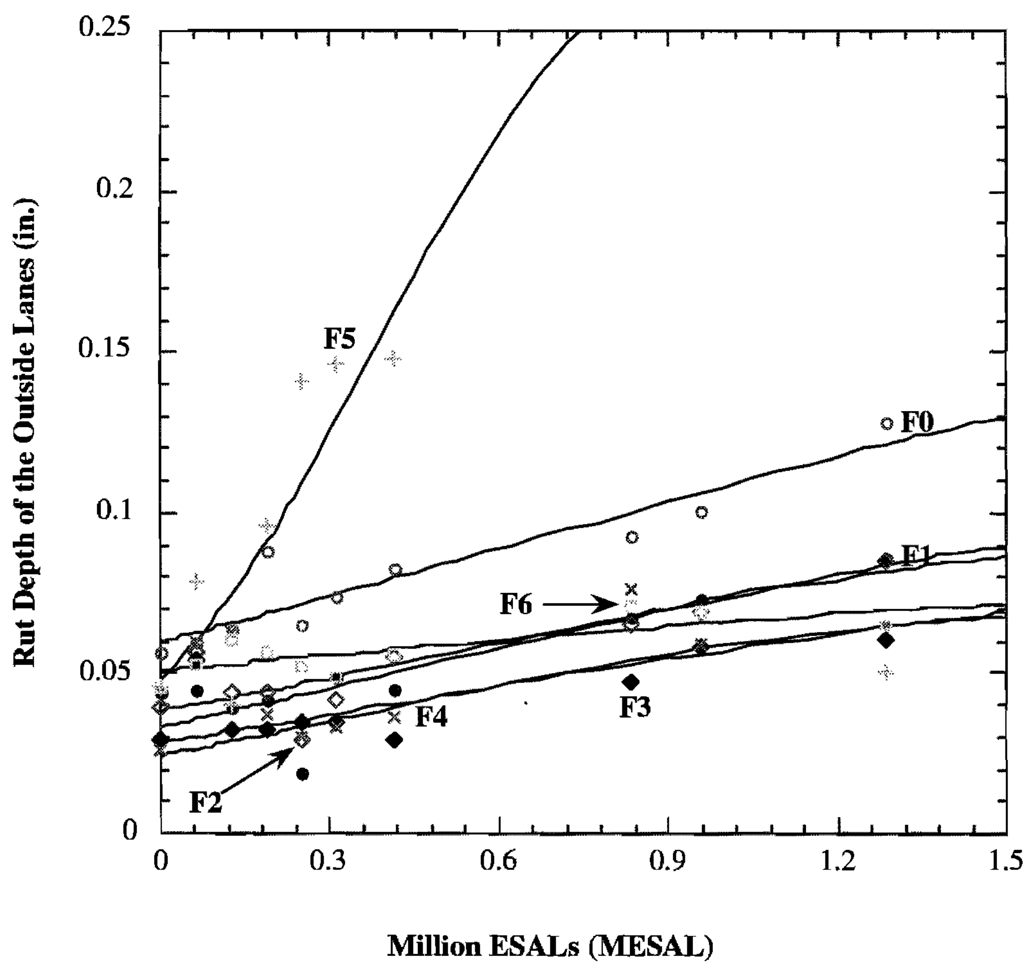

Figure 4.2: Rut depth of the outside lanes of flexible sections

Once again one may apply the logistic equation (Liu and McCullough 1998), namely, Eq (3.2), to obtain the following expressions for the development of rut depth in overlays:

$$
\begin{array}{lll}
\text{F0:} & RD = 0.175\left[1+\exp(0.652-1.14y)\right]^{-1}; & R^2 = 0.88 \\
\text{F1:} & RD = 0.120\left[1+\exp(0.760-1.24y)\right]^{-1}; & R^2 = 0.93 \\
\text{F2:} & RD = 0.100\left[1+\exp(0.703-1.72y)\right]^{-1}; & R^2 = 0.87 \\
\text{F3:} & RD = 0.085\left[1+\exp(0.690-1.43y)\right]^{-1}; & R^2 = 0.90 \\
\text{F4:} & RD = 0.075\left[1+\exp(0.730-2.01y)\right]^{-1}; & R^2 = 0.96 \\
\text{F5:} & RD = 0.300\left[1+\exp(1.655-4.40y)\right]^{-1}; & R^2 = 0.94 \\
\text{F6:} & RD = 0.090\left[1+\exp(-0.27-0.75y)\right]^{-1}; & R^2 = 0.60
\end{array}
\qquad (4.1)
$$

where the rut depth is measured in the right lane, y is the MESAL that has been applied to the right wheelpath, and the statistical R^2 values are shown for each section. Similar results can be obtained for the overlays on rigid sections:

$$
\begin{aligned}
&\text{R0:} && RD = 0.072\,[1+\exp(1.10-2.83y)]^{-1}; && R^2 = 0.80 \\
&\text{R1:} && RD = 0.140\,[1+\exp(1.35-0.81y)]^{-1}; && R^2 = 0.68 \\
&\text{R2:} && RD = 0.235\,[1+\exp(0.93-1.77y)]^{-1}; && R^2 = 0.93 \\
&\text{R3:} && RD = 0.220\,[1+\exp(0.62-2.68y)]^{-1}; && R^2 = 0.99 \\
&\text{R4:} && RD = 0.120\,[1+\exp(0.61-1.18y)]^{-1}; && R^2 = 0.88 \\
&\text{R5:} && RD = 0.073\,[1+\exp(0.12-1.94y)]^{-1}; && R^2 = 0.79 \\
&\text{R6:} && RD = 0.052\,[1+\exp(0.06-2.25y)]^{-1}; && R^2 = 0.82
\end{aligned}
\tag{4.2}
$$

One may notice that the limits of the rut depth are quite low for both overlays on rigid and on flexible pavement. This shows that the development of rut depth of a relatively new pavement is not progressive, which may not be the case when a pavement becomes old and when several types of distress appearing in an overlay become severe. We suspect that there may exist a double or a multistep logistic curve for the development of rut depth for a pavement structure; the verification of this would require a longer observation period.

For practical purposes, one may still fit the data in the fourteen tables above using a linear model, namely,

$$S = ay+b \tag{4.3}$$

to the existing data in Tables 4.1–4.12, so long as fatigue cracking has not become severe in the overlays; a and b are the regression coefficients that can be derived easily from the data, and y is millions of ESALs.

CHAPTER 5. DEVELOPING A REHABILITATION PLAN

INTRODUCTION

The cracking and rutting distress models suggested by Dorman and others are calibrated and presented in this chapter. The terminal failure loadings associated with the cracking and rutting distress appearing in the test sections in the Lufkin District are estimated using the traffic information provided by Dr. Lee and his students (see CTR Report 987-5). The decreasing rate of PSI with respect to the thickness of an overlay for a particular recipe is estimated by observing that the terminal loading associated with the PSI criterion increases linearly with the thickness of the overlays for different overlay recipes. Moreover, the conceptual basis for selecting an optimal rehabilitation plan is illustrated using a simple diagram.

OVERLAYS ON FLEXIBLE PAVEMENTS

The rutting of the flexible pavements is known to depend on the vertical strain on the subgrade according to a power law, with the magnitude of the power ranging somewhere from 4 to 5 (Monismith, 1992). Here, the formula suggested by Dorman is (Cho 1996) is

$$N_{f,r} = \left(\frac{\varepsilon_{v,0}}{\varepsilon_v}\right)^{4.471} \tag{5.1}$$

where $N_{f,r}$ is the terminal ESAL associated with the rut depth of 10.16 mm (0.4 in.), ε_v is the vertical strain on the interface between the overlay and the existing pavement, and $\varepsilon_{v,0}$ is a calibration constant.

It is known that the development of fatigue cracking on a flexible pavement depends on the tensile strain exerted along the interface between the overlay and the overlaid pavement, according to a power law (Pell 1973, Elliot and Thompson 1985). The magnitude of the power falls approximately in the range from 2.5 to 3.5, depending on the failure criterion. The prediction formula for cracking of the flexible pavements suggested is given by (Kennedy 1983):

$$N_{f,c} = \left(\frac{\varepsilon_{t,0}}{\varepsilon_t}\right)^{2.76} \tag{5.2}$$

where $N_{f,c}$ is the terminal ESAL associated with the maximum numbers of cracks allowed on an overlay, ε_t is the tensile strain on the interface between the overlay and the existing pavement, and $\varepsilon_{t,0}$ is a constant. The constant vertical strain $\varepsilon_{v,0}$ and constant tensile strain $\varepsilon_{t,0}$ are calibrated by knowing the quantities $N_{f,r}$ and $N_{f,c}$, which can be estimated using the traffic WIM data provided by Report 987-5.

The theoretical estimate for the tensile and compressive strains for an overlay on flexible sections is obtained using ELSYM 5. In order to use ELSYM 5, we assign Poisson ratios for the asphalt layer, the flexible black base, the cement-treated layer, and the soil layer as 0.40, 0.35, 0.25, and 0.35, respectively. The traffic loading is represented by a circular loading of 453 kg (9,000 lb) with a pressure of 689 kPa (100 psi). The parameters for using Eqs. (5.1) and (5.2) for the overlays on the flexible sections in Project 987 are in Table 5.1.

Table 5.1: The physical parameters for the flexible test sections.

	F0	**F1**	**F2**	**F3**	**F4**	**F6**
Do	3.00	3.00	3.00	3.00	3.00	9.00
Dt	14.00	14.00	14.00	14.00	14.00	9.00
Db	4.50	4.50	4.50	4.50	4.50	4.50
Dc	6.00	6.00	6.00	6.00	6.00	6.00
Ds	infinity	infinity	infinity	infinity	infinity	infinity
Eo	0.40	0.48	0.38	0.42	0.40	0.44
Eb	0.17	0.25	0.18	0.44	0.31	0.16
Ec	0.61	0.70	0.64	0.90	0.79	0.21
Ms	0.02	0.01	0.02	0.02	0.02	0.01

The quantities D_0, D_t, D_b, D_c, D_s (in unit of inches), E_o, E_b, E_c, and M_s (in units of million psi) in Table 5.1 represent the thickness of the present overlay, the total thickness of the overlays, the thickness of flexible black base, the thickness of the cement-treated base, and the thickness of the soil bed; and then the elastic modulus for the surface layer, the modulus for the flexible black base, the modulus for the cement-treated base, and the modulus for the soil layer, respectively. Assuming the failure criteria for cracking and rutting are 5% of the total surface area and 10.16 mm (0.4 in.), respectively, the vertical ($\varepsilon_{v,0}$) and tensile ($\varepsilon_{t,0}$) strain constants are determined as listed in Table 5.2. In general, these constants depend on the magnitudes of the rutting and cracking criteria. This is taken into account when a program code is generated for the overlays on flexible pavements.

Table 5.2: Terminal loadings for cracking and rutting distress for flexible pavements.

	F1	F2	F3	F4	F6
$N_{f,r}$ (MESAL)	13.60	12.80	15.52	9.18	11.17
$\varepsilon_{V,0}$ x 10^6	32.72	39.09	27.47	29.81	74.29
ε_V x 10^6	16.66	18.58	13.06	16.00	53.07
$N_{f,c}$ (MESAL)	13.84	71.92	7.28	3.78	2.87
$\varepsilon_{t,0}$ x 10^6	59.44	118.81	37.29	35.79	97.73
ε_t x 10^6	22.94	25.24	18.17	22.11	66.68

OVERLAYS ON RIGID PAVEMENTS

The theoretical estimate for the tensile and compressive strains for an overlay on a rigid pavement will be obtained using the plane strain model developed by Cho et al. (CTR 1994). For the overlays on rigid pavements, the following formula for tensile strain is used:

$$\ln(\varepsilon_t) = -8.564 - 0.1327D_0 - 1.06E_0 + 0.09949w_e \qquad (5.3)$$

$$\ln(\varepsilon_v) = -6.3291 - 0.1625D_0 - 0.72E_0 + 0.09937w_e \qquad (5.4)$$

where D_0 is the thickness of an overlay in inches, E_0 is the Young's modulus of the overlay in million psi, and w_e is the traffic load in kilopounds. For convenience, we take w_e as the standard 80-kN (18-kip) axle load. The parameters for using Eqs. (5.3) and (5.44) for all the overlays on the rigid section in Project 987 are listed in Table 5.3.

Table 5.3: The physical parameters for the rigid test sections.

	R0	R1	R2	R3	R4	R5	R6
Do	3.00	4.00	5.50	3.00	7.50	4.50	3.00
Eo (R.L.)	0.50	0.34	0.39	0.51	0.31	0.25	0.27
Eo (L.L.)	0.48	0.33	0.32	0.48	0.22	0.17	0.21

The prediction formula for rutting of the flexible overlays is found as

$$N_{f,r} = \left(\frac{\varepsilon_{v,0}}{\varepsilon_v} \right)^{0.735} \tag{5.5}$$

where the exponent 0.735 is found by the observational results from the test sections.

The prediction formula for the cracking of the flexible overlays on rigid pavements is given by

$$N_{f,c} = \left(\frac{\varepsilon_{t,0}}{\varepsilon_t} \right)^{2.76} \tag{5.6}$$

Using Eqs. (5.3) and (5.4), we simplify the Eqs. (5.5) and (5.6) as

$$N_{f,r} = a_R e^{0.1195 D_o} \tag{5.7}$$

and

$$N_{f,c} = a_C e^{0.3663 D_o} \tag{5.8}$$

where the quantities a_R and a_C are in units of MESAL, and D_o is the thickness of an overlay in inches. Assuming the failure criteria for cracking and rutting are 5% and 10.16 mm (0.4 in.), respectively, the quantities a_R and a_C are determined as listed in Table 5.4. In general, these constants depend on the magnitudes of the rutting and cracking criteria. This is taken into account when a program code is generated for the overlays on rigid pavements.

Table 5.4: Terminal loadings for cracking and rutting distress for rigid pavement.

	R0	**R1**	**R4**	**R5**	**R6**
$N_{f,r}$ (MESAL)	8.68	13.74	10.15	17.84	25.71
a_r	6.06	8.52	4.14	10.42	17.96
$N_{f,c}$ (MESAL)	12.85	1.55	2.87	3.77	9.14
a_c	4.28	0.36	0.18	0.73	3.05

SERVICEABILITY CRITERION

The PSI data associated with the outside lane of the rigid or flexible test sections collected for the last 4 years are tabulated in Table 5.5 and Table 5.6, respectively. In addition, the total traffic loadings are listed in both tables in terms of millions of ESALs (MESAL). The information for sections R2, R3, F0, and F5 is not presented in the tables, since these overlay strategies are not recommended for future rehabilitation of US 59 (Cho et al. 1994).

Table 5.5: PSI associated with the outside lane of the rigid sections.

Tm	R0	R1	R2	R3	R4	R5	R6	MESAL
0.000	4.320	4.290	4.580	4.540	4.350	4.360	4.550	0.000
0.250	4.260	4.040	3.610	3.990	4.170	4.330	4.370	0.071
0.750	4.210	3.960	3.950	3.370	3.830	4.290	4.260	0.212
1.500	4.010	3.750	2.560	3.820	4.160	4.190	4.230	0.425
1.750	4.000	3.870	2.670	4.120	4.190	4.300	4.140	0.495
3.583	3.813	3.303	2.265	3.930	4.265	4.178	4.025	1.014
4.500	3.800	2.940	1.930	3.900	3.810	4.050	3.530	1.274

Table 5.6: PSI associated with the outside lane of the flexible sections.

Tm	F0	F1	F2	F3	F4	F6	MESAL
0.000	4.760	4.720	4.730	4.440	4.530	4.500	0.000
0.750	4.750	4.770	4.750	4.430	4.480	4.590	0.212
1.500	4.670	4.660	4.670	4.430	4.520	4.460	0.425
1.750	4.620	4.620	4.620	4.360	4.340	4.290	0.495
3.333	4.387	4.692	4.605	4.400	4.400	2.235	0.944
4.250	4.330	4.490	4.630	4.260	4.440	3.910	1.203

Using the traffic information provided in Report 987-5, one can estimate the terminal loadings associated with the PSI criterion (PSI=2.5). These loadings are shown in Table 5.7. By plotting the terminal loadings associated with different overlay recipes against the thickness of the overlays, one sees a linear trend in the plot. Thus, an empirical linear relationship between the terminal loading for an overlay and the thickness of the overlay may be used, namely

$$N_{f,\mathrm{PSI}} = a_{\mathrm{PSI}}\, D_O\,, \qquad (5.7)$$

where D_O is the thickness of the overlay in inches and a is the coefficient to be calibrated.

Table 5.7: Terminal loadings for PSI for both rigid and flexible pavements.

	R0	R1	R4	R5	R6
$N_{f, PSI}$ (MESAL)	2.70	2.03	10.28	8.71	2.95
a_{PSI}	0.9	0.508	1.37	1.936	0.983
	F1	**F2**	**F3**	**F4**	**F6**
$N_{f, PSI}$ (MESAL)	10.18	10.18	16.57	8.03	5.49
a_{PSI}	3.39	3.39	3.68	2.68	0.61

SELECTING A REHABILITATION STRATEGY

In Figure 5.1, we have drawn a conceptual diagram determined by the rutting and cracking criteria and the PSI criterion. All curves increase monotonically with respect to the thickness of an overlay. It is known that the chances of the three curves intersecting at a point are slim; in such a case, the intersection(s) of the three curves would be the optimal solution(s). For a given thickness *h* of an overlay, the least number derived from the criteria will be the terminal loading for the overlay. For example, the numbers N_1, N_2, and N_3 are the terminal loadings for the selected overlay thicknesses D_1, D_2, and D_3, respectively. For a particular overlay plan, the life-cycle cost depends not only on the above criteria, but also on the total traffic loadings for the selected overlay period, say, 20 years, and user costs. The optimal overlay plan is then selected among all the possible overlay plans in terms of minimal cost. This can be achieved by developing a computer code.

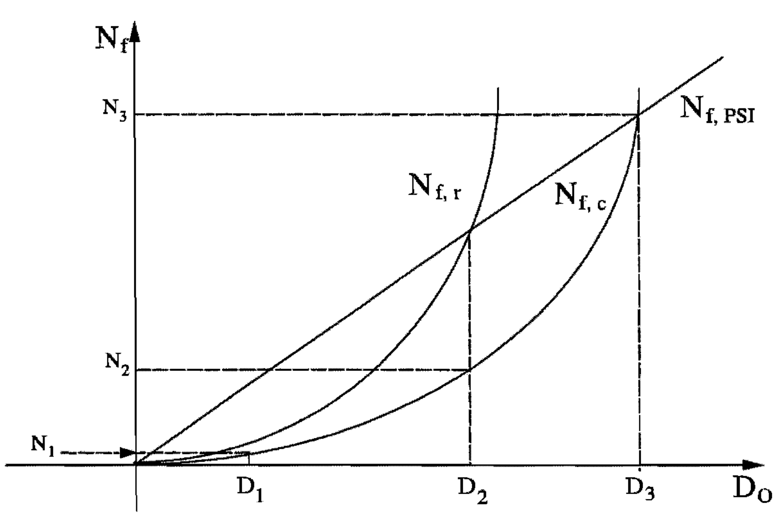

Figure 5.1: Conceptual diagram determined by rutting and cracking criteria and PSI criterion.

The following describes the ten-step calculation for the cost and thickness of an overlay for a particular strategy.

1. Initialize the program.

2. Input the information:
   - ADDT and growth rate,
   - Criterion for cracks,
   - Criterion for rut depth,
   - The Young's modulus for base, subbase, and soil layer,
   - The thickness of different layers (in inches) for the existing pavement, and
   - The cost for the overlays per inch per 1,000 feet and some other costs for each recipe.

3. Calibrate the crack model: Using the Young's modulus for the surface layer for the overlay (from Report 987-4), calculate the model parameter for a mechanistic model using the criterion given in step 2.

4. Calibrate the rut model: Using the Young's modulus for the surface layer for the overlay (from Report 987-4), calculate the model parameter for Dorman's model using the criterion given in step 2.

5. Start with an overlay having a thickness of 12.7 mm (0.5 in.).
6. For a given overlay thickness, *D0,* calculate the terminal loading associated with the given crack rut criteria in step 2, namely, $N_{F,c}$ and $N_{f,r}$, respectively. The terminal loading $N_{f,\ PSI}$ associated with PSI estimated from the test section results is provided in Project 987 tech memos in terms of the overlay thickness, *D0.*

7. Select the minimum values N_f from $N_{f,c}$, $N_{f,r}$, and $N_{f,\ PSL}$

8. Calculate the time for overlaying a pavement for the next *x* years for the terminal loading N_f .
   - Calculate the cost for each overlay.
   - Calculate the total cost for the *x*-year period.
   - Record the above results.

9. Increase the thickness of the overlay by 12.7 mm (0.5 in.) for each overlay.
   - Get out of the loop if a 254-mm (10-in.) overlay for each overlay is reached.
   - Go to step 6.

10. Find the minimum total cost for the overlay strategy with the overlay thickness, *ho,* for each overlay among the above results.
    - Print out the time for the overlay.
    - Print out the cost for each overlay.
    - Print out the total cost for the next x-year rehabilitation period.

DEMONSTRATION USING THE GENERATED COMPUTER CODE

Consider a flexible section having moduli of 3.447 MPa (500 ksi), 4,136 MPa (600 ksi), and 96.5 MPa (14 ksi) for the base, cement-treated base, and subbase layer, respectively. The length of the section, the AADT, and the growth rate for the section are assumed to be: 3.22 km (2 miles), 13,600, 3.96%, respectively. The construction costs given in CTR Report 987-3 for the test sections provide the data used in the following calculations. Denoting *COST (i),* and *Do (i) TIME (i)* as the cost for the *i*th overlay, the thickness of the *i*th overlay, and the time for the *i*th overlay, we run the flexible program for a rehabilitation for a 20-year period and obtain the results shown in Table 5.8.

It is clear that both recipes F3 and F6 are not the favorites in this case; but recipes F1 and F2 may be applied to overlay the section. Considering the development of the reflective cracks in the pavement surface, one may choose the recipe F2 instead of F1. It is expected that both F1 and F2 should perform well, since the asphalt cement is SBS-polymer blended. One may apply F4 under special circumstances.

Consider a rigid section with a length of 3.22 km (2 miles), an AADT Of 13,600, and an annual traffic growth rate of 3.96%. Denoting *COST (i),* and *Do (i) TIME (i)* as the cost for the *i*th overlay, the thickness of the *i*th overlay, and the time for the *i*th overlay, we run the rigid program for a rehabilitation period of 20 years and obtain the results shown in Table 5.9.

It is clear that both recipes R1 and R4 are expensive; but recipes R0, R5, and R6 may be applied to overlay the rigid sections. However, the traditional recipe R0 is the best choice among the three in this situation.

Table 5.8: Construction cost for a 3.22-km (2-mile) long flexible section using different recipes.

	F1	**F2**	**F3**	**F4**	**F6**
TIME(1)	0.00	0.00	0.00	0.00	0.00
Do(1)	1.50	1.50	1.50	2.00	4.00
COST(1)	175,555	178,374	151,858	201,707	432,358
TIME(2)	14.89	14.89	8.97	12.94	8.21
Do(2)	2.00	2.00	2.00	2.50	5.00
COST(2)	133,189	135,360	145,441	144,114	393,019
TIME(3)	26.13	26.13	15.30	23.36	15.01
Do(3)			3.50		6.00
COST(3)			189,127		357,251
TIME(4)			21.53		21.27
TOTAL COST ($)	308,744	313,735	486,426	345,821	1,182,628

Table 5.9: Construction cost for a 3.22-km (2-mile) long rigid section using different recipes.

	R0	**R1**	**R4**	**R5**	**R6**
TIME(1)	0.00	0.00	0.00	0.00	0.00
Do(1)	3.00	4.50	6.50	2.00	3.00
COST(1)	177,852	1,203,725	744,218	253,834	302,681
TIME(2)	8.95	7.76	8.21	9.60	9.64
Do(2)	3.50	5.50	7.00	2.50	3.50
COST(2)	151,614	985,882	576,879	219,276	246,333
TIME(3)	15.79	14.12	14.74	17.05	16.90
Do(3)	4.50	7.00	7.50	3.00	4.00
COST(3)	148,132	830,291	482,064	190,133	212,781
TIME(4)	22.53	20.41	20.84	23.74	23.17
TOTAL COST	477,597	3,019,897	1,803,161	663,243	761,795

CHAPTER 6. OVERLAY STRATEGIES

The overlay strategies for different control sections of US 59 in the Lufkin District are found using the optimization program (see Chapter 5) and given in the last two columns of the following tables for the SNAPS counties in the district. Three numbers are placed in a parentheses, namely, (x, y, z); the first number is the thickness of the overlay, the second is the time for overlaying a pavement section, and the third is the agency cost for overlaying the section. The first overlay is assumed to be in place by the year 2000.

The first project in Shelby County, i.e., control 63 section 06, would have 51 mm (2 in.), 64 mm (2.5 in.), 76 mm (3 in.), and 89 mm (3.5 in.) thick overlays during the years 2000, 2012, 2025, and 2040, respectively. The present value of these overlays (i.e., year 2000) are \$110,000, \$89,000, \$64,000, and \$42,000, respectively. These combinations were determined by the optimization program used to minimize life-cycle cost based on the net present value of each overlay. A discount rate of 0.4% annually was used in the analysis. The increase in thickness for each subsequent overlay is a result of traffic growth projections as given by the growth rate columns in the table. Optimal overlay thicknesses were rounded to the nearest 12.7 mm (0.5 in.), partly for reasonableness of construction, and partly to compensate for any small amount of necessary milling of the existing surface. Other columns in the tables use the terms defined below:

C.S.	Control section (TxDOT)
B.M.	Starting distance form beginning of C.S.
E.M.	Ending distance from beginning of C.S.
B.R.M.	Beginning reference marker
E.R.M.	Ending reference marker
AADT 1994	Average annual daily traffic (1994)
N.B.	Composition of existing pavement northbound lane
S.B.	Composition of existing pavement southbound lane
Growth rate	AADT annual growth rate, percent

Tables 6.1 through 6.5 report the optimal strategies for US 59 rehabilitation as determined by the optimization program described in Chapter 5. In reality, there is no one, unique, optimal solution for problems of this sort. However, the values given here are believed to be reasonable approximations that, when applied with engineering judgment, will yield the desired years of service at the least cost. Moreover, all of these solutions rely on the accuracy of the traffic prediction models, which are based on limited data (as mentioned previously in this report and documented in detail in Report 987-7 of this series).

The correct application of the distress models developed in Chapter 5 depends on the detailed traffic information collected from different US 59 locations. The strategies given in the following tables are obtained assuming the composition of traffic along US 59 is the same as the composition of traffic in the detecting site, since no further traffic information is available or was recorded in terms of vehicle type and weight. The AADT detected at the test sections is approximately 7,500, with 25% of the AADT coming from all types of trucks (i.e., the test sections are frequently used by heavy vehicles). The AADT for some locations along US 59 is high — over 30,000 in some cases. One may question whether the truck composition is still as high as 25% of the total traffic; in our estimation this seems unlikely for all the locations. Overestimating percent trucks can lead to an expensive overlay strategy, as shown in the table for Angelina County.

Table 6.1: Recommended overlay strategies for US 59 in Shelby Co.

Shelby										
C.S.	B.M.	E.M.	B.R.M.	E.R.M.	AADT 1994	NB	SB	Growth Rate (%)	NB	SB
63-06	0.000	1.851	326	326	7500	R9	F1	0.585	(2", 0.0,110k); (2.5",11.9, 89k,); (3.0", 24.8, 64k); (3.5", 39.4, 42k).	(1", 0.0,113k); (1.5",15.5, 92k,); (2.0", 29.6,70k); (2.5", 43.3, 50k)
175-2	0.000	1.412	328	328	5900	R?	R?	-2.900	(1.5", 0., 63k,); (2.0",12.1, 52k); (2.5", 27.2, 36k); (3.0", 46.4, 21k)	(1.5", 0., 63k,); (2.0",12.1, 52k); (2.5", 27.2, 36k); (3.0", 46.4, 21k)
175-4	1.412	6.486	328	336	6000	R11	R11	0.893	(1.5", 0., 226k,); (2.0",10.8, 203k); (2.5", 23.0,153k); (3.0", 37.0,110k)	(1.5", 0., 226k,); (2.0",10.8, 203k); (2.5", 23.0,153k); (3.0", 37.0,110k)
	6.486	7.696	336	336	5900	R11	R11	0.182	(1.5", 0., 54k,); (2.0",11.9, 47k); (2.5", 26.3, 32k); (3.0", 44.1, 19k)	(1.5", 0., 54k,); (2.0",11.9, 47k); (2.5", 26.3, 32k); (3.0", 44.1, 19k)
	7.696	8.361	336	336	6000	R11	R11	-1.820	(1.5", 0., 30k,); (2.0",11.9, 26k); (2.5", 26.8, 18k); (3.0", 45.6, 10k)	(1.5", 0., 30k,); (2.0",11.9, 26k); (2.5", 26.8, 18k); (3.0", 45.6, 10k)
	8.361	8.776	336	338	6600	R11	R11	-0.386	(1.5", 0., 18.5k,); (2.0",10.8, 16.6k); (2.5", 24.2, 12.0k); (3.0", 41.3, 7.4k)	(1.5", 0., 18.5k,); (2.0",10.8, 16.6k); (2.5", 24.2, 12.0k); (3.0", 41.3, 7.4k)
175–5	0.121	0.464	338	338	8700	F4	F4	0.340	(1", 0.0,19.9k); (1.5",8.8, 21.2k,); (2", 16.8,20.3k); (2.5", 24.9,18.4k); (?, 33.2,?)	(1", 0.0,19.9.0k); (1.5",8.8, 21.2k,); (2", 16.8,20.3k); (2.5", 24.9,18.4k); (?, 33.2,?)
	0.464	0.789	338	338	8300	F4	F4	1.411	(1", 0.0,21.0k); (1.5",8.8, 22.4k,); (2", 15.5,21.5k); (2.5", 22.1,20.0k); (3.5", 28.3,21.8k); (?, 35.0,?)	(1", 0.0,21.0k); (1.5",8.8, 22.4k,); (2", 15.5,21.5k); (2.5", 22.1,20.0k); (3.5", 28.3,21.8k); (?, 35.0,?)
	0.789	2.090	338	340	7100	F4	F4	1.614	(1", 0.0,79.5k); (1.5",9.5, 81.5k,); (2", 17.3, 78.2k); (2.5", 24.3, 73.6k) ; (?,31.0,?)	(1", 0.0,79.5k); (1.5",9.5, 81.5k,); (2", 17.3, 78.2k); (2.5", 24.3, 73.6k) ; (?,31.0,?)
	2.090	5.308	340	342	6200	R13	R13	0.657	(1.5", 0., 143k,); (2".0",10.7, 129k); (2.5", 23.1, 97k); (3.0", 37.6, 67k)	(1.5", 0., 143k,); (2".0",10.7, 129k); (2.5", 23.1, 97k); (3.0", 37.6, 67k)

Table 6.2: Recommended overlay strategies for US 59 in Nacogdoches Co.

Nacogdoches										
C.S.	B.M.	E.M.	B. R. M.	E. R. M.	AADT 1994	NB	SB	Growth Rate (%)	NB	SB
175-6	0.000	1.463	346	346	6700	R	R	1.86	(2.5", 0.0, 108k); (3.0",14.2, 75k,); (3.5", 27.2, 53k); (4.0", 40.1, 36k)	(2.5", 0.0, 108k); (3.0",14.2, 75k,); (3.5", 27.2, 53k); (4.0", 40.1, 36k)
	1.463	1.600	346	346	7800	R8	R8	-0.57	(2.0", 0.0, 8.1k); (2.5",12.2, 6.3k,); (3.0", 26.5, 4.4k); (3.5", 43.8, 2.7k)	(2.0", 0.0, 8.1k); (2.5",12.2, 6.3k,); (3.0", 26.5, 4.4k); (3.5", 43.8, 2.7k)
	1.600	2.547	346	348	8600	F4?	F4?	1.30	(1", 0.0, 58k); (1.5", 17.5, 43k); (2", 34.3, 29k)	(1", 0.0, 58k); (1.5", 17.5, 43k); (2", 34.3, 29k)
175-7	2.547	2.800	348	348	7500	R8	R8	1.57	(1", 0.0, 15.5k); (1.5",19.1, 10.7k); (2", 36.8, 7k)	(1", 0.0, 15.5k); (1.5",19.1, 10.7k); (2", 36.8, 7k)
	2.800	5.630	348	350	7500	F4	F4	1.57	(1", 0.0,173k); (1.5",12.1, 158k,); (2", 22.1, 140k); (2.5", 31.4,122k); (3.0, 40.1,102k)	(1", 0.0,173k); (1.5",12.1, 158k,); (2", 22.1, 140k); (2.5", 31.4,122k); (3.0, 40.1,102k)
	5.630	11.714	350	356	7500	F4	F4	1.10	(1", 0.0,372.2k); (1.5",11.6, 352k,); (2", 21.6, 313k); (2.5", 31.1, 261.9 k); (3", 40.3, 220 k)	(1", 0.0,372.2k); (1.5",11.6, 352k,); (2", 21.6, 313k); (2.5", 31.1, 261.9 k); (3", 40.3, 220 k)
	11.714	16.145	356	360	8600	F4	F4	1.80	(1", 0.0,271.1k); (1.5",9.7, 277.7k,); (2", 17.5, 266.6k); (2.5", 24.6, 251.0k); (3.5, 31.1, 264.3k)	(1", 0.0,271.1k); (1.5",9.7, 277.7k,); (2", 17.5, 266.6k); (2.5", 24.6, 251.0k); (3.5, 31.1, 264.3k)
2560-1	1.990	3.196	362	362	13600	F4	F1	3.98	(1.5", 0.0, 108k); (2.0", 9.3, 99k,); (3.5", 16.1, 130k); (4.5", 22.8, 131k); (6.0", 29.3, 132k); (?, 36.1, ?)	(1.5", 0.0, 108k); (2.0", 9.3, 99k,); (3.5", 16.1, 130k); (4.5", 22.8, 131k); (6.0", 29.3, 132k); (?, 36.1, ?)
	3.196	4.905	362	364	19700	F4	F1	4.75	(2.5", 0.0, 248k); (5.5", 7.1, 407k,); (7.0", 20.4, 408k); (8.5", 27.2, 375k); (9.5", 33.8, 319k)	(2.5", 0.0, 248k); (5.5", 7.1, 407k,); (7.0", 20.4, 408k); (8.5", 27.2, 375k); (9.5", 33.8, 319k)

Table 6.2: Recommended overlay strategies for US 59 in Nacogdoches Co., cont.

Nacogdoches										
C.S.	B.M.	E.M.	B. R. M.	E. R. M.	AADT 1994	NB	SB	Growth Rate (%)	NB	SB
2560-1	4.905	7.049	364	366	19100	F4	F1	3.76	(2.0", 0.0, 251k); (4.0", 7.2, 374k,); (5.5", 13.6, 403k); (7.0", 26.7, 389k); (8.0", 33.3, 351k)	(2.0", 0.0, 251k); (4.0", 7.2, 374k,); (5.5", 13.6, 403k); (7.0", 26.7, 389k); (8.0", 33.3, 351k)
	7.049	8.169	366	368	18800	F4	F4	3.93	(2.0", 0.0, 131k); (4.0", 7.4, 195k,); (5.5", 13.8, 211k); (7.0", 20.3, 203k); (8.0", 27.0, 183k)	(2.0", 0.0, 131k); (4.0", 7.4, 195k,); (5.5", 13.8, 211k); (7.0", 20.3, 203k); (8.0", 27.0, 183k)
	8.169	9.027	368	368	19800	F2	F2	4.48	(5.5", 0.0, 269k); (8.0", 7.3, 296k,); (9.5", 13.9, 277k); (11.0", 20.4, 243k); (12.0", 27.2, 202k)	(5.5", 0.0, 269k); (8.0", 7.3, 296k,); (9.5", 13.9, 277k); (11.0", 20.4, 243k); (12.0", 27.2, 202k)
	9.027	9.795	368	368	17260	F2	F2	3.88	(1.5", 0.0, 68.5k); (2.0", 9.5, 63k,); (3.0", 16.5, 71k); (4.5", 23.0, 80k); (5.5", 29.9, 77k); (?, 36.7, ?)	(1.5", 0.0, 68.5k); (2.0", 9.5, 63k,); (3.0", 16.5, 71k); (4.5", 23.0, 80k); (5.5", 29.9, 77k); (?, 36.7, ?)
176-1	23.781	26.000	368	370	25000	F1	F1	2.75	(2.5", 0.0, 322k); (6.0", 7.1, 576k,); (8.0", 13.7, 604k); (10.0", 20.4, 573k); (11.5.", 27.5, 500k); (?, 34.9, ?)	(2.5", 0.0, 322k); (6.0", 7.1, 576k,); (8.0", 13.7, 604k); (10.0", 20.4, 573k); (11.5.", 27.5, 500k); (?, 34.9, ?)
	26.000	27.300	370	372	25000	R7	F4	2.75	(5.5", 0., 212k); (6.0", 8.2, 169k,); (6.5", 14.8, 145k); (7.5", 21.0, 127k); (8.5", 27.5, 114k); (9.0", 34.1, 91k)	(2.5", 0.0, 189k); (6.0", 7.1, 337k,); (8.0", 13.7, 354k); (10.0", 20.4, 335k); (11.5.", 27.5, 293k); (?, 34.9, ?)
	27.300	29.970	372	376	25000	R7	R6	2.75	(5.5", 0.0, 424k); (6.0", 8.2, 338k,); (6.5", 14.8, 289k); (7.5", 21.0, 254k); (8.5", 27.5, 227k); (9.0", 34.1, 183k)	(5.5", 0.0, 424k); (6.0", 8.2, 338k,); (6.5", 14.8, 289k); (7.5", 21.0, 254k); (8.5", 27.5, 227k); (9.0", 34.1, 183k)
	29.970	32.894	376	378	19300	R6	R6	2.94	(4.5", 0.0, 390k); (5.0", 8.5, 317k,); (5.5", 15.4, 265k); (6.0", 22.0, 228k); (7.0", 28.3, 202k); (7.5", 35.1, 165k)	(4.5", 0.0, 390k); (5.0", 8.5, 317k,); (5.5", 15.4, 265k); (6.0", 22.0, 228k); (7.0", 28.3, 202k); (7.5", 35.1, 165k)

Table 6.3: Recommended overlay strategies for US 59 in Angelina Co.

Angelina										
C.S.	B.M.	E.M.	B. R. M.	E. R. M.	AADT 1994	NB	SB	Growth Rate (%)	NB	SB
176-2	0.000	1.232	378	380	19300	F4	R6	2.45	(4.0", 0., 146k); (4.5", 7.9, 125k); (5.0", 14.7, 105k); (5.5", 21.3, 88k); (6.0", 27.8, 76k); (6.5", 34.2, 63k)	(4.0", 0., 146k); (4.5", 7.9, 125k); (5.0", 14.7, 105k); (5.5", 21.3, 88k); (6.0", 27.8, 76k); (6.5", 34.2, 63k)
	1.232	2.900	380	380	22000	R6	R6	2.57	(5.0", 0., 247k); (5.5", 8.5, 199k); (6.0", 15.6, 165k); (6.5", 22.3, 136k); (7.0", 28.7, 115k); (8.0", 35.0, 100k)	(5.0", 0., 247k); (5.5", 8.5, 199k); (6.0", 15.6, 165k); (6.5", 22.3, 136k); (7.0", 28.7, 115k); (8.0", 35.0, 100k)
	2.900	4.600	382	382	22000	R8,6	R8,6	2.29	(4.5", 0., 227k); (5.0", 7.9, 191k); (5.5", 14.6, 165k); (6.0", 21.2, 133k); (6.5", 27.6, 114k); (7.0", 34.0, 97k)	(4.5", 0., 227k); (5.0", 7.9, 191k); (5.5", 14.6, 165k); (6.0", 21.2, 133k); (6.5", 27.6, 114k); (7.0", 34.0, 97k)
	4.600	6.033	384	384	22000	R4?	R4?	2.06	(4.5", 0., 191k); (5.0", 8.1, 155k); (5.5", 15.0, 135k); (6.0", 21.8, 112k); (6.5", 28.5, 92k); (7.0", 35.2, 75k)	(4.5", 0., 191k); (5.0", 8.1, 155k); (5.5", 15.0, 135k); (6.0", 21.8, 112k); (6.5", 28.5, 92k); (7.0", 35.2, 75k)
2553-1	9.976	11.543	386	387	22000	R9	R9	5.32	(5.5", 0., 255k); (7.0", 7.7, 247k); (9.0", 14.2, 241k); (10.5", 21.0, 214k), (12.5", 27.7, 201k); (14.0", 34.5, 171k)	(5.5", 0., 255k); (7.0", 7.7, 247k); (9.0", 14.2, 241k); (10.5", 21.0, 214k), (12.5", 27.7, 201k); (14.0", 34.5, 171k)
	11.543	12.467	387	388	30000	R6	R6	7.52*	(6.0", 0., 164k); (8.5", 7.6, 177k); (11.5", 14.3, 182k); (14.0", 21.3, 168k); (17.0", 28.3, 155k); (20.0", 35.4, 139k)	(6.0", 0., 164k); (8.5", 7.6, 177k); (11.5", 14.3, 182k); (14.0", 21.3, 168k); (17.0", 28.3, 155k); (20.0", 35.4, 139k)
	12.467	12.687	388	388	30000	R6	R6	5.96*	(6.0", 0., 36k); (7.5", 7.9, 34k); (10.0", 14.3, 34k); (12.0", 21.2, 31k); (14.0", 28.1, 28k); (26.0", 35.0, 25k)	(6.0", 0., 36k); (7.5", 7.9, 34k); (10.0", 14.3, 34k); (12.0", 21.2, 31k); (14.0", 28.1, 28k); (26.0", 35.0, 25k)
	12.687	13.230	388	389	27510	R6	R6	4.58	(6.5", 0., 105k); (8.0", 7.7, 98k); (10.0", 14.1, 93k); (10.0", 14.1, 93k); (11.5", 20.9, 84k); (13.5", 27.5, 75k); (15",34.2, 64k)	(6.5", 0., 105k); (8.0", 7.7, 98k); (10.0", 14.1, 93k); (10.0", 14.1, 93k); (11.5", 20.9, 84k); (13.5", 27.5, 75k); (15",34.2, 64k)
	13.230	14.131	389	390	32000	R6	R6	5.88*	(6.5", 0., 174k); (8.5", 8.0, 166k); (10.5", 14.1, 162k); (12.5", 21.5, 147k); (15.0", 28.3, 134k); (17.0", 35.2, 115k)	(6.5", 0., 174k); (8.5", 8.0, 166k); (10.5", 14.1, 162k); (12.5", 21.5, 147k); (15.0", 28.3, 134k); (17.0", 35.2, 115k)

Table 6.3: Recommended overlay strategies for US 59 in Angelina Co., cont.

Angelina										
C.S.	B.M.	E.M.	B. R. M.	E. R. M.	AADT 1994	NB	SB	Growth Rate (%)	NB	SB
2553-1	14.131	14.831	390	390	33000	R6	R6	6.32*	(6.5", 0., 135k); (8.5", 7.7, 134k); (11.0", 14.2, 132k); (13.5", 21.0, 128k); (16.0", 27.8, 115k); (18.5", 34.7, 115k)	(6.5", 0., 135k); (8.5", 7.7, 134k); (11.0", 14.2, 132k); (13.5", 21.0, 128k); (16.0", 27.8, 115k); (18.5", 34.7, 115k)
	14.831	15.900	390	391	32530	R6	R6	5.73*	(6.5", 0., 206k); (8.0", 7.9, 193k); (10.5", 14.3, 192k); (12.5", 21.2, 174k); (14.5", 27.9, 159k); (17.0", 34.7, 142k)	(6.5", 0., 206k); (8.0", 7.9, 193k); (10.5", 14.3, 192k); (12.5", 21.2, 174k); (14.5", 27.9, 159k); (17.0", 34.7, 142k)
176-3	1.240	3.202	391	392	40000	R4	R6	3.55*	(8.0", 0., 465k); (8.5", 8.4, 361k); (10", 14.7, 336k); (11.5", 21.2, 293k); (13", 27.6, 262k); (14.5", 34.1, 222k)	(8.0", 0., 465k); (8.5", 8.4, 361k); (10", 14.7, 336k); (11.5", 21.2, 293k); (13", 27.6, 262k); (14.5", 34.1, 222k)
	3.202	6.568	392	394	24000	R4	R6	3.77	(5.5", 0., 549k); (6.5", 7.9, 493k); (7.5", 14.5, 432k); (8.5", 20.9, 387k); (10", 27.3, 346k); (11", 33.9, 301k)	(5.5", 0., 549k); (6.5", 7.9, 493k); (7.5", 14.5, 432k); (8.5", 20.9, 387k); (10", 27.3, 346k); (11", 33.9, 301k)
	6.568	7.664	394	396	25000	R4	R6	3.58	(5.5", 0., 179k); (6.5", 7.7, 160k); (7.5", 14.2, 141k); (8.5", 20.6, 126k); (10", 26.9, 117k); (11", 33.6, 98k)	(5.5", 0., 179k); (6.5", 7.7, 160k); (7.5", 14.2, 141k); (8.5", 20.6, 126k); (10", 26.9, 117k); (11", 33.6, 98k)
	7.664	9.221	396	398	24000	R6	R4	2.12	(5.0", 0., 231k); (5.5", 8.2, 185k); (6.0", 15.1, 154k); (6.5", 21.8, 132k); (7", 28.4, 108k); (7.5", 349, 91k)	(5.0", 0., 231k); (5.5", 8.2, 185k); (6.0", 15.1, 154k); (6.5", 21.8, 132k); (7", 28.4, 108k); (7.5", 349, 91k)
	9.221	10.420	398	398	23000	R4	R6	1.89	(4.5", 0., 160k); (5.0", 7.9, 135k); (5.5", 14.6, 113k); (6.0", 21.4, 94k); (6.5", 28.1, 77k); (7", 34.7, 66k)	(4.5", 0., 160k); (5.0", 7.9, 135k); (5.5", 14.6, 113k); (6.0", 21.4, 94k); (6.5", 28.1, 77k); (7", 34.7, 66k)
	10.420	10.738	398	400	21000	R4	R6	1.57	(5.5", 0., 52k); (6.0", 10.6, 38k); (6.5", 19.7, 29k); (7", 28.6, 39k); (7.5", 37.2, 17k)	(5.5", 0., 52k); (6.0", 10.6, 38k); (6.5", 19.7, 29k); (7", 28.6, 39k); (7.5", 37.2, 17k)
	10.738	11.278	400	400	19700	R4	R6	2.37	(4.5", 0., 72k); (5", 8.7, 58k); (5.5", 16.0, 47k); (6", 23.1, 39k); (6.5", 30.0, 32k); (7", 36.7, 27k)	(4.5", 0., 72k); (5", 8.7, 58k); (5.5", 16.0, 47k); (6", 23.1, 39k); (6.5", 30.0, 32k); (7", 36.7, 27k)
	11.278	12.683	400	402	16700	R4	R6	2.51	(5.5", 0., 208k); (5.5", 11.0, 149k); (6.0", 20.0, 119k); (6.5", 28.4, 90k); (7", 36.4, 71k)	(5.5", 0., 208k); (5.5", 11.0, 149k); (6.0", 20.0, 119k); (6.5", 28.4, 90k); (7", 36.4, 71k)

Table 6.4: Recommended overlay strategies for US 59 in Polk Co.

Polk										
C.S.	B.M.	E.M.	B. R. M.	E. R. M.	AADT 1994	NB	SB	Growth Rate (%)	NB	SB
176-4	0.000	2.548	404	406	16700	R2	R2	3.82	(4.0", 0.0, 302k); (4.5", 8.2, 248k,); (5.5", 14.6, 240k); (6.5", 21.4, 215k); (7.0", 28.3, 176k); (8.0", 34.8, 159k)	(4.0", 0.0, 302k); (4.5", 8.2, 248k,); (5.5", 14.6, 240k); (6.5", 21.4, 215k); (7.0", 28.3, 176k); (8.0", 34.8, 159k)
	2.548	7.714	406	406	17500	R2	R2	3.19	(4.0", 0.0, 612k); (4.5", 8.2, 504k,); (5.0", 14.9, 442k); (6.0", 21.3, 403k); (6.5", 28.0, 332k); (7.5", 34.6, 303k)	(4.0", 0.0, 612k); (4.5", 8.2, 504k,); (5.0", 14.9, 442k); (6.0", 21.3, 403k); (6.5", 28.0, 332k); (7.5", 34.6, 303k)
	7.714	8.562	412	412	17400	R2	R2	2.89	(4.0", 0.0, 101k); (4.5", 8.4, 83k,); (5.0", 15.4, 70k); (5.5", 22.1, 58k); (6.0", 28.6, 50k); (7.0", 35.0, 46k)	(4.0", 0.0, 101k); (4.5", 8.4, 83k,); (5.0", 15.4, 70k); (5.5", 22.1, 58k); (6.0", 28.6, 50k); (7.0", 35.0, 46k)
	8.562	9.073	412	412	19100	R2	R2	1.61	(5.0", 0.0, 76k); (5.5", 10.5, 56k,); (6.0", 19.7, 43k); (6.5", 28.6, 33k); (7.0", 37.4, 25k)	(5.0", 0.0, 76k); (5.5", 10.5, 56k,); (6.0", 19.7, 43k); (6.5", 28.6, 33k); (7.0", 37.4, 25k)
	9.073	9.481	412	412	18200	R2	R2	0.20	(3.5", 0.0, 42k); (4.0", 9.0, 35k,); (4.5", 18.1, 27k); (5.0", 28.2, 20k); (5.5", 39.4, 15k)	(3.5", 0.0, 42k); (4.0", 9.0, 35k,); (4.5", 18.1, 27k); (5.0", 28.2, 20k); (5.5", 39.4, 15k)
176-5	9.481	10.481	412	414	16100	R3	R3	0.36	(3.0", 0.0, 89k); (3.5", 8.6, 76k,); (4.0", 17.3, 61k); (4.5", 27.6, 46k); (5.0", 37.7, 35k)	(3.0", 0.0, 89k); (3.5", 8.6, 76k,); (4.0", 17.3, 61k); (4.5", 27.6, 46k); (5.0", 37.7, 35k)
	10.481	14.015	414	418	15100	R3	R3	2.42	(4.5", 0.0, 471k); (5.0", 11.0, 340k,); (5.5", 20.2, 263k); (6.0", 28.8, 210k); (6.5", 37.1, 160k)	(4.5", 0.0, 471k); (5.0", 11.0, 340k,); (5.5", 20.2, 263k); (6.0", 28.8, 210k); (6.5", 37.1, 160k)
	14.015	14.807	418	418	14800	R3	R3	1.81	(4.0", 0.0, 94k); (4.5", 10.7, 71k,); (5.0", 20.0, 54k); (5.5", 29.2, 41k); (6.0", 38.2, 32k)	(4.0", 0.0, 94k); (4.5", 10.7, 71k,); (5.0", 20.0, 54k); (5.5", 29.2, 41k); (6.0", 38.2, 32k)
	14.807	15.551	418	418	15600	R3	R3	3.23	(4.0", 0.0, 92k); (4.5", 9.1, 73k,); (5.0", 16.4, 61k); (5.5", 23.3, 51k); (6.0", 30.0, 42k)	(4.0", 0.0, 92k); (4.5", 9.1, 73k,); (5.0", 16.4, 61k); (5.5", 23.3, 51k); (6.0", 30.0, 42k)

Table 6.4: Recommended overlay strategies for US 59 in Polk Co., cont.

Polk										
C.S.	B.M.	E.M.	B. R. M.	E. R. M.	AADT 194	NB	SB	Growth Rate (%)	NB	SB
176-5	15.551	21.800	418	424	15100	R3	R3	2.70	(3.5", 0.0, 648k); (4.0", 8.6, 541k,); (4.5", 15.9, 463k); (5.0", 23.1, 376k); (5.5", 30.1, 314k)	(3.5", 0.0, 648k); (4.0", 8.6, 541k,); (4.5", 15.9, 463k); (5.0", 23.1, 376k); (5.5", 30.1, 314k)
	21.800	22.336	424	426	17100	R3	R3	3.17	(4.0", 0.0, 64k); (4.5", 8.4, 52k,); (5.0", 15.2, 44k); (5.5", 21.7, 38k); (6.5", 28.0, 34k); (7.0", 34.8, 29k)	(4.0", 0.0, 64k); (4.5", 8.4, 52k,); (5.0", 15.2, 44k); (5.5", 21.7, 38k); (6.5", 28.0, 34k); (7.0", 34.8, 29k)
	22.400	25.877	426	428	15800	R3	R3	2.78	(3.5", 0.0, 361k); (4.0", 8.2, 301k,); (4.5", 15.1, 258k); (5.0", 22.0, 226k); (5.5", 28.6, 189k); (6.0", 35.3, 157k)	(3.5", 0.0, 361k); (4.0", 8.2, 301k,); (4.5", 15.1, 258k); (5.0", 22.0, 226k); (5.5", 28.6, 189k); (6.0", 35.3, 157k)
	25.877	28.800	428	432	16800	R3	R3	2.70	(4.0", 0.0, 347k); (4.5", 8.8, 285k,); (5.0", 16.2, 231k); (5.5", 23.3, 231k); (6.0", 30.2, 193k)	(4.0", 0.0, 347k); (4.5", 8.8, 285k,); (5.0", 16.2, 231k); (5.5", 23.3, 231k); (6.0", 30.2, 193k)
	28.800	29.215	432	432	16800	F1	F1	2.70	(1.5", 0., 37.0k); (2.0",7.9, 37.0k); (3.5", 14.0, 50.1k); (5.0", 20.0, 56.2k); (7.0", 26.0, 59.5k); (?, 33.,?)	(1.5", 0., 37.0k); (2.0",7.9, 37.0k); (3.5", 14.0, 50.1k); (5.0", 20.0, 56.2k); (7.0", 26.0, 59.5k); (?, 33.,?)
	29.215	30.500	432	432	15400	F1	F1	3.96	(1.5", 0., 114.6 k); (3.0",7.8, 169.2k); (5.5", 13.9, 241.8k); (7.5", 20.3, 249.4k); (7.5", 26.5, 249k); (?, 33., ?)	(1.5", 0., 114.6 k); (3.0",7.8, 169.2k); (5.5", 13.9, 241.8k); (7.5", 20.3, 249.4k); (7.5", 26.5, 249k); (?, 33., ?)
	30.500	31.300	432	432	15400	R?	R?	3.96	(4.0", 0.0, 95k); (4.5", 8.7, 78k,); (5.0", 15.5, 66k); (6.0", 21.8, 62k); (7.0", 28.5, 55k); (7.5", 35.3, 45k)	(4.0", 0.0, 95k); (4.5", 8.7, 78k,); (5.0", 15.5, 66k); (6.0", 21.8, 62k); (7.0", 28.5, 55k); (7.5", 35.3, 45k)
177-1	31.372	33.084	432	432	16810	F1	F1	2.52	(1.5", 0., 152.7 k); (2.0",8.4, 169.2k); (2.5", 15.0, 143.6k); (3.0", 21.1, 130.1k); (3.5", 26.9, 124.3k); (?, 33., ?)	(1.5", 0., 152.7 k); (2.0",8.4, 169.2k); (2.5", 15.0, 143.6k); (3.0", 21.1, 130.1k); (3.5", 26.9, 124.3k); (?, 33., ?)
	33.084	33.331	432	432	23000	F1	F1	2.04	(2.5", 0., 35.9 k); (3.5", 7.2, 37.8 k); (4.5", 13.3, 38.2k); (5.5", 19.5, 36.7k); (6.0", 25.9, 31.6k); (?, 32.3,?)	(2.5", 0., 35.9 k); (3.5", 7.2, 37.8 k); (4.5", 13.3, 38.2k); (5.5", 19.5, 36.7k); (6.0", 25.9, 31.6k); (?, 32.3,?)
	33.331	36.000	432	438	19500	F1	F1	3.00	(2.5", 0., 38.8 k); (4.5", 7.1, 52.2 k); (5.5", 13.6, 50.2k); (6.5", 20.0, 46.8k); (8.0", 26.2, 43.6k); (?, 32.3,?)	(2.5", 0., 38.8 k); (4.5", 7.1, 52.2 k); (5.5", 13.6, 50.2k); (6.5", 20.0, 46.8k); (8.0", 26.2, 43.6k); (?, 32.3,?)
	36.000	37.693	438	440	19500	R?	R?	3.00	(4.5", 0., 226 k); (5.0", 8.4, 183 k); (5.5", 15.2, 153 k); (6.5", 21.6, 143 k); (7.0", 28.5, 117k); (7.5", 35.0, 99k)	(4.5", 0., 226 k); (5.0", 8.4, 183 k); (5.5", 15.2, 153 k); (6.5", 21.6, 143 k); (7.0", 28.5, 117k); (7.5", 35.0, 99k)
	37.693	38.609	440	442	21000	F3	F3	3.96	(3.0", 0., 159 k); (5.0", 7.2, 199 k); (6.5", 13.6, 203k); (8.0", 20.0, 197k); (9.0", 26.6, 168k); (?", 33.2, ?)	(3.0", 0., 159 k); (5.0", 7.2, 199 k); (6.5", 13.6, 203k); (8.0", 20.0, 197k); (9.0", 26.6, 168k); (?", 33.2, ?)
	38.609	39.496	442	442	18000	F3	F3	2.59	(2.5", 0., 128.8 k); (4.0", 7.2, 154.5 k); (5.0", 13.5, 152.0k); (6.0", 19.7, 143.7k); (7.0", 25.9, 132.2 k); (?, 32.2,?)	(2.5", 0., 128.8 k); (4.0", 7.2, 154.5 k); (5.0", 13.5, 152.0k); (6.0", 19.7, 143.7k); (7.0", 25.9, 132.2 k); (?, 32.2,?)
	39.496	41.565	442	444	18500	R	R	2.50	(4.0", 0., 245 k); (4.5", 8.2, 202k); (5.0", 15.1, 170k); (5.5", 21.9, 148k); (6.0", 28.6, 123k); (6.5", 35.1, 101k)	(4.0", 0., 245 k); (4.5", 8.2, 202k); (5.0", 15.1, 170k); (5.5", 21.9, 148k); (6.0", 28.6, 123k); (6.5", 35.1, 101k)

Table 6.5: Recommended overlay strategies for US 59 in San Jacinto Co.

San Jacinto										
C.S.	B.M.	E.M.	B. R. M.	E. R. M.	AADT 1994	NB	SB	Growth Rate (%)	NB	SB
177-2	0.000	4.291	444	450	19800	F1	F1	2.90	(1.5", 0.0,383k); (2.5", 7.8, 474k,); (4.0", 14.2, 568k); (5.0", 20.8, 559k); (6", 27.4, 508k); (6.5", 34.0, 418k)	(1.5", 0.0,383k); (2.5", 7.8, 474k,); (4.0", 14.2, 568k); (5.0", 20.8, 559k); (6", 27.4, 508k); (6.5", 34.0, 418k)
	4.291	5.143	450	450	18700	F1	F1	2.71	(2.5", 0.0, 124k); (4", 7.2, 148k,); (5.5", 13.5, 160k); (6.5", 20.1, 144k); (7.5", 26.6, 131k); (8", 33.1, 106k)	(2.5", 0.0, 124k); (4", 7.2, 148k,); (5.5", 13.5, 160k); (6.5", 20.1, 144k); (7.5", 26.6, 131k); (8", 33.1, 106k)
	5.143	5.534	450	450	19500	F1	F1	1.84	(2.0", 0.0,46k); (3.5", 7.1, 60k,); (4.0", 13.5, 54k); (5", 19.7, 53k); (5.5", 26.0, 46k); (6.5, 32.1, 41k)	(2.0", 0.0,46k); (3.5", 7.1, 60k,); (4.0", 13.5, 54k); (5", 19.7, 53k); (5.5", 26.0, 46k); (6.5, 32.1, 41k)
	5.534	7.400	450	452	20000	F1	F1	2.13	(2.5", 0.0,271k); (4", 7.1, 325k,); (5", 13.4, 320k); (6", 19.8, 302k); (6.5", 26.3, 249k); (7.5", 32.5, 226k)	(2.5", 0.0,271k); (4", 7.1, 325k,); (5", 13.4, 320k); (6", 19.8, 302k); (6.5", 26.3, 249k); (7.5", 32.5, 226k)
	7.400	19.850	452	456	20000	F2	F2	2.00	(3", 0.0, 2157k); (4", 7.3, 2169k,); (5", 13.4, 2133k); (6", 19.6, 2017k); (7", 26.0, 1856k); (7.5, 32.4, 1510k)	(3", 0.0, 2157k); (4", 7.3, 2169k,); (5", 13.4, 2133k); (6", 19.6, 2017k); (7", 26.0, 1856k); (7.5, 32.4, 1510k)
	19.850	23.216	456	458	20000	F2	F2	1.67	(2.5", 0.0, 489k); (3.5", 7.1, 515k,); (4.5", 13.3, 520k); (5", 19.7, 456k); (6", 25.8, 431k); (6.5", 32.2, 354k)	(2.5", 0.0, 489k); (3.5", 7.1, 515k,); (4.5", 13.3, 520k); (5", 19.7, 456k); (6", 25.8, 431k); (6.5", 32.2, 354k)

CHAPTER 7. SUMMARY, CONCLUSIONS, AND RECOMMENDATIONS

SUMMARY

In Chapter 1, we briefly described Project 987 and reported what we intend to do in the future for US 59. In Chapter 2, we organized US 59 traffic data in terms of TxDOT classified sections, the pavement types defined previously in CTR Report 987–1, and mile markers along the roadway. In Chapter 3, a general logistic model for the development of reflective cracks in pavement surface is proposed and verified using the information collected for the last eight conditions surveys of the test sections. Also, the area of fatigue cracking in the test sections was estimated using field information. In Chapter 4, the rut depth data relating to the wheelpaths in various test sections were found to follow the Gamma distribution. The raw average rut depth for various test sections was plotted against the amount of traffic loading placed on the pavement. The irregular behavior of the rut data was observed for various test sections during the first 2-year period. In Chapter 5, analytic models predicting the development of reflective cracks, fatigue cracks, and rut depth in pavement surfaces were selected and calibrated using the field data. Then, two computer programs, one for flexible pavement and the other for rigid pavement, were developed for the future rehabilitation of US 59. Examples using the programs were demonstrated and reasonable results were obtained. In Chapter 6, overlay strategies for different control sections along US 59 were proposed based on the AADT information collected in the past, which may not be adequate for road sections with high traffic volume (e.g., an AADT of 30,000 or more). Note that the AADT for the test sections is about 7,500. This is primarily due to the fact that the overall truck composition of US 59 is unlikely to be as high as the percentage recorded at the test site, which was about 25%. Seeking a proper overlay strategy requires decomposing a high AADT in terms of vehicle types and weight, as was done by the WIM station in the test site.

FINDINGS AND CONCLUSIONS

Using traffic information and falling weight deflectometer (FWD) data collected from different locations along US 59 within the Lufkin District, and developing descriptive models for cracking and rutting distress using the observational results collected from the test sections, we have identified the optimal rehabilitation plan for US 59.

Regarding the cracking and rutting behavior in pavement overlays, the following conclusions are drawn:

(1) The development of the number of cracks in overlays was found to follow the known logistic curve. The method may be extended to a pavement surface without overlays.

(2) The development of the area of fatigue cracking in overlays was found to follow the known logistic curve. The method may be extended to a pavement surface without overlays.

(3) The development of the rut depth in overlays was found to follow the known logistic curve.

(4) A means for explaining the initial rate of cracking was found by superimposing the rate of initial cracking on top of the logistic process.

(5) A general model was proposed and solved by including specific functions for the initial rate of cracking. It would be interesting to know the general functional form of the initial rate of cracking.

(6) It was found that the time for maximum rate of cracking is equivalent to approximately 0.5 million ESALs for the flexible overlays on rigid pavement and 0.8 million ESALs for the flexible overlays on flexible pavement. Are these observations true in general?

(7) It was found that the time it takes a surface pattern to evolve from 10% cracks to 90% of the maximum number of cracks is equivalent to approximately 0.6 million ESALs for flexible overlays on both rigid pavement and flexible pavement (except for sections R3, F1, and F2). Section R3 was set up with 203 mm (8 in.) Arkansas mix to retard reflection cracks, and the time equivalent for section R3 was found to be 0.9 million ESALs. The time equivalents for both polymer-modified flexible sections F1 and F2 were found to be 0.85 and 2.0 million ESALs, respectively. The polymer-modified AC does resist reflective cracks and other types of cracking.

(8) Overlays R0, R1, R2, and R6, which were directly placed on the previously existing rigid pavement, showed a fast initial growth of reflection cracks. Moreover, overlays R3, R4, and R5, which were not placed directly on the original existing surface, showed a lag phase in the development of reflection cracks. It is clearly unwise to place a layer of flexible pavement on top of a cracked surface without treating the existing surface, since proper treatment is needed to retard the propagation of reflective cracking.

(9) It was found that all the overlays on flexible pavement showed a lag phase in the development of reflection cracks.

(10) It was found that rut depth in pavement overlays fluctuates considerably in the first 2 years and then exhibits a linear growth phase. This fluctuation is expected to some extent for a new asphalt overlay. It is expected that the rut depth will go into a stable phase and develop slowly with time, though the verification of this is beyond the current monitoring period of this project (Thompson and Nauman 1993). A longer observational period is necessary to understand the rutting behavior of overlays; another important question pertains to the length of the stable period.

(11) It was found that the rut depths follow the Gamma distribution quite well. More research is needed to understand why.

(12) It was found that the rut depth for most test sections is low and ranges from 2.54 mm (0.1 in.) to 5.08 mm (0.2 in.). Thus, rut depth is not progressive for a relatively new overlay on a properly designed pavement structure.

Regarding the numerical program developed for the US 59 rehabilitation plan, the following conclusions are drawn:

(1) It was found that the program provides reasonable results for the time and the thickness of each overlay in a rehabilitation of 30 years or more for road sections having present traffic volumes less than 25,000 AADT, and with an annual growth rate less than 3%. The problem here is not with the model but with the incomplete traffic information provided. The model is calibrated using an AADT of 7,500 (collected in the test section), of which 25% of the traffic is comprised of all types of trucks. This leads to the question of whether a road section on US 59 within the Lufkin District serving, say, 400,000 AADT, actually sustains 100,000 various types of trucks a day. This appears unlikely. An exact answer can be provided only through additional WIM station data, which are not available at this time.

(2) The model can be applied to other road sections in US 59 outside of the Lufkin District.

(3) The recipe R0 is found to be the most "economical" recipe for overlaying rigid pavements, and F2 for overlaying flexible pavements in the Lufkin District.

RECOMMENDATIONS

Rehabilitation plans for different road sections of US 59 within the Lufkin District have been generated based on the empirical distress models developed and calibrated using the observational results collected from the test sections over a period of 4.5 years. Many questions and problems encountered in developing the plan remain to be answered and investigated. The recommendations for future research are described below.

(1) The logistic curve was found to accurately describe cracking and rutting distress. The questions are: How long an observation period is needed in order to generate a "correct" prediction from the curve? and: Does there exist a multistep logistic curve for describing the cracking and rutting distress?

(2) There are many existing software package for backcalculating Young's modulus for each layer of a multilayer pavement structure. The results provided by these packages can be dramatically different.

(3) Continuing to monitor the test sections (i.e., keeping the WIM station) and undertaking more observations of cracking and rutting distress appearing in the

pavement surface are important for understanding the distress models developed in this report.

(4) It would be useful to collect the historical data and the future data to develop a history of longitudinal distress appearing in the overlay surfaces.

(5) For better estimation of traffic ESAL loading, more WIM stations should be installed along US 59 within the Lufkin District. Collecting accurate traffic information is crucial for understanding the pavement distress and pavement deteriorations, and also for providing better designs and rehabilitation strategies in the future.

REFERENCES

Hoskins, B. E., B. Frank McCullough, and David Fowler (1991). "The Development of a Long-Range Rehabilitation Plan for US 59 in District 11–Preliminary Report," Research Report CTR 987-1, Center for Transportation Research, The University of Texas at Austin.

Allison, Brent T., and B. Frank McCullough (1994). "Construction of Rehabilitation Test Sections on US 59 in the Lufkin District," Research Report CTR 987-3, Center for Transportation Research, The University of Texas at Austin.

Chartrand, A. (1977). *Introductory Graph Theory,* Dover Publications Inc., New York.

Cho, Yoon-Ho, J. Weissmann, and B. Frank McCullough (1994). "Initial Performance of Asphalt Overlays on Overlaid Jointed Concrete Pavement (JCP) and on Flexible Pavements in Field Test Sections in Lufkin, Texas." Research Report CTR 987-4, Center for Transportation Research, The University of Texas at Austin.

Cho, Yoon-Ho, C. Liu, T. Dossey, and B. Frank McCullough (1994). "Comparisons and Investigations of Some Rehabilitation Strategies Using an FEM for Rigid Pavements in the Lufkin District." Research Report CTR 987-7, Center for Transportation Research, The University of Texas at Austin.

Cho, Yoon-Ho (1996). "Asphalt Overlay Design Methods for Rigid Pavement Considering Rutting, Cracking, Reflection Cracking, and Fatigue Cracking." Doctoral dissertation, The University of Texas at Austin.

Elliot, R. P., and R. Marshall Thompson (1985). "ILLI–PAVE Mechanistic Analysis of AASHO Road Test Flexible Pavements." *Transportation Research Record* 1354, TRB, National Research Council, Washington, D.C.

Finn, Fred N., and Carl L. Monismith (1984). "Asphalt Overlay Design Procedures." *NCHRP Synthesis of Highway Practice* No. 116, Transportation Research Board, National Research Council, Washington, D.C.

Kennedy, Thomas W. (1983). "Tensile Characterization of Highway Pavement Materials." Research Report 183-15F, Center for Transportation Research, The University of Texas at Austin.

Lee, Clyde E., and K. Ahmad Safry (1993). "Effects of Work Zone Detours on Rural Highway Traffic Operations." Research Report CTR 987-2, Center for Transportation Research, The University of Texas at Austin.

Lee, Clyde E., and Joseph E. Garner (1997). "Collection and Analysis of Augmented Weigh-in-Motion Data." Research Report CTR 987-8, Center for Transportation Research, The University of Texas at Austin.

Lee, Clyde E., and Jeffrey W. Pangburn (1996). "Preliminary Research Findings on Traffic-Load Forecasting Using Weigh-in-Motion Data." Research Report CTR 987-5, Center for Transportation Research, The University of Texas at Austin.

Hoskins, Brock E., B. F., McCullough, and David W. Fowler (1989). "The Development of a Long-Range Rehabilitation Plan for US 59 in District 11—Preliminary Report." Research Report CTR 987-1, Center for Transportation Research, The University of Texas at Austin.

Liu, Chiu, R. Herman, and B. Frank, McCullough. "An Investigation of the Development of Cracks on Pavement Overlays," *Proceedings of 1996 International Road Federation Asia-Pacific Regional Meeting.*

Liu, Chiu, T. Dossey, and B. Frank, McCullough. "Final Report on the Long-Range Rehabilitation Plan for US 59 in the Lufkin District," Research Report CTR 987-9, Center for Transportation Research, The University of Texas at Austin.

Monismith, Carl L. (1992). "Analytically Based Asphalt Pavement Design and Rehabilitation: Theory to Practice, 1962-1992." *Transportation Research Record 1354,* Transportation Research Board, Washington, D.C., 5-26.

Montroll, E. W., and W. W. Badger (1974). *Introduction to Quantitative Aspects of Social Phenomena,* Gordon and Breach Science Publisher, New York.

Pell, P. S. (1973). "Structural Design of Asphalt Concrete Pavement Systems to Prevent Fatigue Cracking." *Special Report 140,* HRB, National Research Council, Washington, D.C.

Pell, P. S. (1969). "Fatigue Characteristics of Bitumen and Bituminous Mixes." *Proceedings,* International Conference on the Structural Design of Asphalt Pavement, University of Michigan.

Qu, Tongbin. (1997). "Analysis of Weigh-in-Motion Data for Forecasting Traffic Loads." Master's thesis, The University of Texas at Austin.

Qu, Tongbin, Clyde E. Lee, and Huang Liren (1997). "Traffic-Load Forecasting Using Weigh-in-Motion Data." Research Report CTR 987-6, Center for Transportation Research, The University of Texas at Austin.